Three-Dimensional Modeling for Functional Analysis of Cardiac Images: A Review

Alejandro F. Frangi*, *Student Member, IEEE*, Wiro J. Niessen, *Associate Member, IEEE*, and Max A. Viergever

Invited Paper

***Abstract*—Three-dimensional (3-D) imaging of the heart is a rapidly developing area of research in medical imaging. Advances in hardware and methods for fast spatio-temporal cardiac imaging are extending the frontiers of clinical diagnosis and research on cardiovascular diseases.**

In the last few years, many approaches have been proposed to analyze images and extract parameters of cardiac shape and function from a variety of cardiac imaging modalities. In particular, techniques based on spatio-temporal geometric models have received considerable attention. This paper surveys the literature of two decades of research on cardiac modeling. The contribution of the paper is three-fold: 1) to serve as a tutorial of the field for both clinicians and technologists, 2) to provide an extensive account of modeling techniques in a comprehensive and systematic manner, and 3) to critically review these approaches in terms of their performance and degree of clinical evaluation with respect to the final goal of cardiac functional analysis. From this review it is concluded that whereas 3-D model-based approaches have the capability to improve the diagnostic value of cardiac images, issues as robustness, 3-D interaction, computational complexity and clinical validation still require significant attention.

***Index Terms*—Cardiac imaging, functional analysis, model-based image analysis.**

NOMENCLATURE

n-D	n-dimensional, $n \in \{2,3,4\}$.
nDE	n-dimensional echocardiography.
BA	Biplane angiography.
c	Curvedness.
CDT	Continuous distance transform.
CFM	Color flow (Doppler) mapping.
CI	Cardiac index.
CO	Cardiac output.
CSG	Constructive solid geometry.
CT	Computed tomography.
CVD	Cardiovascular disease.
DOFs	Degrees of freedom.
DSR	Dynamic spatial reconstructor.
E	Green's strain tensor.
EBCT	Electron beam computed tomography.
EDV	End diastolic volume.
EF	Ejection fraction.
ESV	End systolic volume.
F	Deformation gradient tensor.
FE	Finite element.
FFD	Free-form deformation.
$\gamma(h,t)$	Shape spectrum.
GCG	Geometric cardiogram.
GDT	Geometrically deformable template.
H	Mean curvature.
HARP	Harmonic phase.
HR	Heart rate.
ICP	Iterative closest point (algorithm).
K	Gaussian curvature.
k_1, k_2	Principal curvatures.
KLT	Karhunen-Loeve transform.
LV	Left ventricle.
LVM	Left ventricular mass.
LVV	Left ventricular volume.
MF	Wall/tissue motion field.
MRI	Magnetic resonance imaging.
MTI	Model tag intersections.
NN	Neural network.
NURBS	Nonuniform rational B-spline.
RV	Right ventricle.
RVV	Right ventricular volume.
s	Shape index.
SA	Strain analysis.
SPAMM	Spatial modulation of magnetization.
SPECT	Single photon emission computed tomography.
SSP	Similar shape patches.
SV	Stroke volume.
SVI	Stroke volume index.
τ	Local stretching factor.
US	Ultrasound (imaging).
WT	Wall thickening.

Manuscript received April 25, 2000; revised October 5, 2000. This work was supported by the Netherlands Ministry of Economic Affairs under Project IOP Beeldverwerking IBV97009 and by EasyVision Advanced Development, Philips Medical Systems BV, Best, The Netherlands. The Associate Editor responsible for coordinating the review of this paper and recommending its publication was A. Amini. *Asterisk indicates corresponding author.*

*A. F. Frangi is with the Image Sciences Institute (ISI), University Medical Center, Rm E.01.334, Heidelberglaan 100, 3584 CX, Utrecht, The Netherlands (e-mail: alex@isi.uu.nl).

W. J. Niessen and M. A. Viergever are with the Image Sciences Institute (ISI), University Medical Center, Heidelberglaan 100, 3584 CX, Utrecht, The Netherlands.

Publisher Item Identifier S 0278-0062(01)00799-6.

I. Introduction

The number one cause of death in the United States since 1900 in every year but one (1918) has been CVD. More than 2600 Americans die each day of CVD; an average of one death every 33 s [1]. CVD claims more lives each year than the next seven leading causes of death combined. According to the most recent computations of the Centers for Disease Control and Prevention of the National Center for Health Statistics (CDC/NCHS), if all forms of major CVD were eliminated, life expectancy would rise by almost ten years while with elimination of all forms of cancer the gain would be three years [1].[1]

Nowadays, there is a multitude of techniques available for cardiac imaging which provide qualitative and quantitative information about morphology and function of the heart and great vessels (Fig. 1). Use of these technologies can help in guiding clinical diagnosis, treatment, and follow-up of cardiac diseases. Spatio-temporal imaging is a valuable research tool to understand cardiac motion and perfusion, and their relationship with stages of disease.

Technological advances in cardiac imaging techniques provide 3-D information with continuously increasing spatial and temporal resolution. Therefore, a single cardiac examination can result in a large amount of data (particularly in multiphase 3-D studies). These advances have led to an increasing need for efficient algorithms to plan 3-D acquisitions, automate the extraction of clinically relevant parameters, and provide tools for their visualization.

Segmentation of cardiac chambers is an invariable prerequisite for quantitative functional analysis. Although many clinical studies still rely on manual delineation of chamber boundaries, this procedure is time-consuming and prone to intraobserver and interobserver variability. Therefore, many researchers have addressed the problem of automatic LV and RV segmentation. Since the shape of the cardiac ventricles is approximately known, it seems natural to incorporate prior shape knowledge into the segmentation process. Such *model-driven* techniques have received ample attention in medical image analysis in the last decade [3], [4]. A few advantages over model-free approaches are: 1) the model itself can constrain the segmentation process that is illposed in nature owing to noise and image artifacts; 2) segmentation, image analysis and shape modeling are simultaneously addressed in a common framework; 3) models can be coarse or detailed depending on the desired degree of abstraction; 4) in some approaches, most of the chamber's shape can be explained with a few comprehensible parameters which can subsequently be used as cardiac indexes (cf. [5]–[9] among others).

Use of geometric models is not completely new to the analysis of cardiac images. As a matter of fact, traditional methods of obtaining parameters such as LVV and mass from echocardiography and angiocardiography were based on (simple) geometrical models [10]–[13]. However, their use was mainly motivated by the need of extracting 3-D parameters from two-dimensional (2-D) images and their accuracy was, therefore, limited [14].

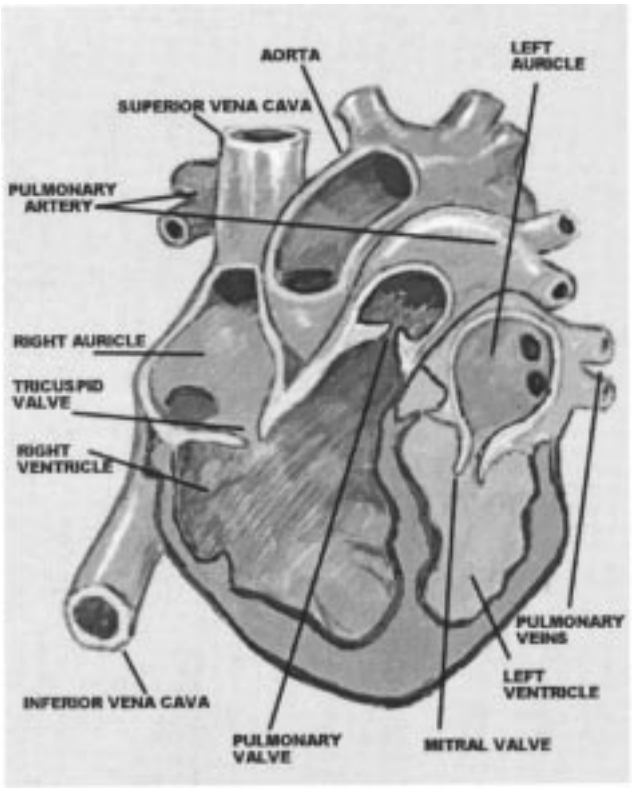

Fig. 1. Diagram of the heart.

The literature on model-driven segmentation of cardiac images has grown rapidly in the last few years and this trend is likely to continue. To the best of our knowledge no survey is available that reviews this work. This paper presents a comprehensive and critical review of the state-of-the-art in geometric modeling of the cardiac chambers, notably the LV, and their potential for functional analysis. In order to set reasonable bounds to the extent of this survey, we have confined ourselves to peer-reviewed *archival publications*[2] proposing methods for LV (RV) segmentation, shape representation, and functional and/or motion analysis, that fulfill the following selection criteria:

- the technique is model-based;
- the reconstructed model is 3-D[3];
- illustration on cardiac images is provided.

This review is organized as follows. Section II gives a brief overview of the different acquisition modalities that have been used in imaging the heart. Section III overviews and defines the most relevant clinical parameters that provide information on cardiac function. Section IV presents a systematic classification of cardiac models by type of geometrical representation/parameterization. Attention is also given to the different types of input data and features for model recovery. This section is summarized in Table I. Section V discusses cardiac modeling ap-

[1]At the time of writing, the authors could not find similar statistics for Europe. There is, however, an ongoing European survey on CVDs whose results are expected to appear soon [2].

[2]A few exceptions were made when the approaches were considered relevant and journal versions were not available.

[3]Even if the imaging technique is not 3-D like, for instance, in the reconstruction of 3-D models from multiple nonparallel slices or from multiple 2-D projections.

TABLE I
OVERVIEW OF CARDIAC MODELING METHODS. SEE KEYS IN FIG. 3

	Reference	Model	Potential	Reported	Type of Input	Type of Feature
Surface Models						
Continuous	Yettram [98, 99]	Stacked curves	BA	BA	M2DP	manual contours
	Young [60, 100]	Bicubic Hermite patches	BA	BA	PS	coronary bifurcation points
	Spinale [101]^{RV}	Stacked hemiellipses	BA	BA	M2DP	manual contours
	Pentland [102]	FE and modal analysis	NS	X	M2DP	optic flow
	Cauvin [103]	Truncated bullet	NS	SPECT	3DV	thresh. + morphol. skeleton
	Czegledy [104]^{RV}	Stack of crescentic outlines	NS	CT	3DV	linear measurements
	Gustavsson [105]	Cubic B-spline curves' mesh	US	US	MO2DS	manual contours
	Sacks [106]^{RV}	Biquadric surface patches	NS	MR	3DV	manual contours
	Chen [107]	Superquadrics + spher. harmon.	NS	BA	PS	coronary bifurcation points
	Denslow [108]^{RV}	Ellipsoidal shell	NS	MR	3DV	linear measurements
	Maehle [29]	Bicubic spline surface patches	NS	US	MO2DS	edge detection + manual correction
	Chen [109]	Voxel repres. / superquadric	NS	DSR	3DV	shape & grey-level properties
	Coppini [27]	Spherical elastic surface	NS	US	MO2DS	NN edge detector
	Goshtasby [110]	Rational Gaussian surface	NS	MR	3DV	zero-crossings Laplacian
	Matheny [111]	3-D/4-D harmonic surfaces	NS	DSR/BA	PS	iso-surface, coronary bifurcation points
	Staib [112]	Bayesian Fourier surface	NS	MR/DSR	3DV	Gaussian gradient
	Park [6]	Superquadrics + par. functions	MR^{tag}	MR^{tag}	PS	MR tagging-derived mid-wall motion field [68]
	Bardinet [9, 113]	Superquadrics + FFD	NS	DSR/SPECT	PS	iso-surfaces
	Declerck [114]	Planispheric transformation	NS	SPECT	3DV	normalized radial gradient
	Sato [115]	B-spline surface	BA	BA	M2DP	apparent/occluding contours
Discrete	Geiser [116, 117]	12-sided stacked polygons	US	US	MO2DS	manual contours
	Faber [118]	4-D discrete template	NS	MR/SPECT	3DV	normalized radial gradient
	Gopal [25]	Polyhedral mesh	NS	US	MO2DS	manual contours
	Friboulet [119]	Triangulated mesh	NS	MR	PS	manual contours
	Huang [120]	Adaptive-size mesh	NS	DSR	PS	data-to-node distance + data curvature
	Faber [121]	3D discrete template	SPECT	SPECT	3DV	radioactive distrib. profile
	Germano [122, 123]	Ellipsoid + local refinement	SPECT	SPECT	3DV	radioactive distrib. profile
	McInerney [124]	FE deformable balloon	NS	DSR	3DV	Gauss/Monga-Deriche grad.
	Ranganath [125]	2D snakes + propagation	MR	MR	3DV	intensity profile matching
	Tu [126]	Spherical template	NS	DSR	3DV	spatio-temporal gradient
	Nastar [127]	Mass-spring mesh	NS	DSR	3DV	edge distance map
	Rueckert [128]	Geom. Def. Template	NS	MR	3DV	zero-crossings Laplacian
	Shi [129, 130]	Delaunay triangulation	NS	MR/DSR	PS	bending energy
	Legget [26]	Piecewise subdivision surface	NS	US	MO2DS	manual contours
	Montagnat [131]	Simplex meshes	US	US	MO2DS	edges in cylindrical coord.
	Biedenstein [132]	Bullet-like elastic mesh	SPECT	SPECT	3DV	radioactive distrib. profile
Implicit	Yezzi [133, 134]	Implicit snakes	NS	MR	3DV	Gaussian gradient
	Tseng [135]	Cont. Dist. Tranf. NN	NS	US	MO2DS	manual contours
	Niessen [136]	Implicit snakes	NS	MR/DSR	3DV	Gaussian gradient
	Lelieveldt [137]	Fuzzy implicit surfaces	CT/MR	MR	MO2DS	air-tissue transitions
Volume Models						
Continuous	Creswell [138, 139]	Approximating NURBS	MR	MR	PS	manual contours
	Park [5]	Superellipsoids + par. functions	MR^{tag}	MR^{tag}	TAG	tag line intersections + boundary points
	Haber [140, 141]	Physics-based FE	MR^{tag}	MR^{tag}	TAG	tag line intersections + boundary points
	Shi [142]	Biomechanical tetrahedral FE model	MR	MR	PS+3DV	bending energy + MR velocity image
Discrete	Kuwahara [143]	Voxel representation	MR	MR	MO2DS	manual contours
	O'Donnell [7, 8]	Hybrid volumetric ventriculoid	MR^{tag}	MR^{tag}	TAG	tag line intersections + boundary points
Deformation Models						
Continuous	Amini [86]	Local quadric patches	NS	DSR/MR	PS	minimal conformal motion
	Young [68]	Bicubic Hermite FE	MR^{tag}	MR^{tag}	TAG	tag line intersections
	Bartels [144]	Multi-dimensional splines	NS	Syn	3DV	intensity conservation
	O'Dell [145]	Affine + prolate spheroidal	MR^{tag}	MR^{tag}	TAG	tag lines
	Young [72]	Bicubic Hermite FE	MR^{tag}	MR^{tag}	TAG	tag lines
	Moulton [146]	Higher-order polyn. interpol.	MR^{tag}	MR^{tag}	TAG	tag surface intersections
	Radeva [147]	Trivariate cubic B-spline	MR^{tag}	MR^{tag}	TAG	short axis tag lines
	Kerwin [74]	Thin-plate splines	MR^{tag}	MR^{tag}	TAG	tag line intersections
	Young [148]	"Model tags"	MR^{tag}	MR^{tag}	TAG	tag lines
	Huang [149]	Four-variated cubic B-spline	MR^{tag}	MR^{tag}	TAG	tag surfaces
Discrete	Moore [69]	Discrete mesh	MR^{tag}	MR^{tag}	TAG	tag line intersections
	Denney [73]	Discrete grid	MR^{tag}	MR^{tag}	TAG	tag line intersections
	Benayoun [90]	Adaptive-size meshes	NS	DSR	3DV	gradient
	Papademetris [150–152]	Delaunay triangulation	NS	MR/US	PS	internal deformation energy

proaches with respect to the functional parameters they provide and the degree of evaluation of these methods. This section leads to Table II that links the clinical target of obtaining functional information of the heart (Section III) to the various technical approaches presented in Section IV. Finally, Section VI closes the survey with conclusions and suggestions for future research.

II. IMAGING TECHNIQUES FOR CARDIAC EXAMINATION

The physical properties on the basis of which the imaging device reconstructs an image (e.g., radioactive emission of an isotope) are intimately related to some specific functional aspects of the heart (e.g., its perfusion properties). Each imaging

Keys to Table I:
Modality: BA = Biplane Angiocardiography; US = Ultrasound, MR = Magnetic Resonance; DSR = Dynamic Spatial Reconstructor; CT = Computed Tomography; X = transmission X-ray; SPECT = Single Photon Emission Computed Tomography; Syn = Synthetic images; NS = Non Specific.
Recovered from: M2DP = multiple 2-D projections; MO2DS = multiple oriented 2-D slices; 3DV = 3-D volumetric images/feature maps; PS = point sets; TAG = MR tag intersections, lines or surfaces.

Fig. 3. Keys to Table I.

modality presents advantages and limitations that influence the achievable modeling accuracy. This section briefly reviews the techniques most frequently used for 3-D clinical investigation of the heart. More extensive reviews and complementary readings can be found in [15]–[22].

A. Angiocardiography

Angiocardiography is the X-ray imaging of the heart following the injection of a radio-opaque contrast medium. Although 2-D in principle, this technique can provide projections from two angles using a biplane system. Selective enhancement of the lesion to be demonstrated can be accomplished by positioning an intravascular catheter through which the contrast medium is guided and injected. Angiocardiography is usually good at anatomic delineation of lesions but much less satisfactory in determining their severity and the degree of hemodynamic disturbance that they have produced. This technique has been used for a long time to assess EF and volumes [10] based on simplified geometric models [11]–[13] of the LV, but most radiologists use visual assessment based on experience [15].

B. Cardiac US

Two-dimensional US of the heart or "echocardiography" [16], [22] allows the anatomy and movements of intracardiac structures to be studied noninvasively. The application of pulsed and continuous-wave Doppler principles to 2-D echocardiography (2DE) permits blood flow direction and magnitude to be derived and mapped onto a small region-of-interest of the 2DE image. In CFM, the pulsed-wave signal with respect to blood velocity and direction of flow throughout the imaging plane is color coded, and produces a color map over the 2DE image. One of the limiting factors of 2DE is the US window (presence of attenuating tissues in the interface between the US transducer and the organ of interest). To overcome this problem *transesophageal echocardiography* can be used, which allows for high-quality color flow images at the expense of being invasive.

Three-dimensional echocardiography (3DE) [17] is a relatively new development in US that allows 3-D quantitation of organ geometry since the complete organ structure can be imaged. This technique has been used to compute LV volume and mass [23]–[28] and to perform wall motion analysis [29].

C. Isotope Imaging

Isotopes have been used to study LV function and myocardial perfusion. Radionuclide techniques for monitoring global and regional ventricular function fall into two major categories: 1) *first-pass studies* in which the injected bolus dose is monitored during its first passage through the heart and great vessels and 2) *gated equilibrium studies*, in which the tracer mixes with the blood pool before data collection. First pass acquisitions are typically 2-D, while gated equilibrium studies can be 2-D or 3-D (SPECT). Isotope imaging can be used to assess parameters like EF [30] and regional wall motion analysis [30]–[32]. It is also used to study myocardial perfusion [33] in cases of ischemia or myocardial infarction, and to assess myocardial viability. The overwhelming majority of radionuclide studies performed for perfusion assessment are SPECT.

D. Cardiac CT

Conventional CT [19] had virtually no place in cardiovascular examinations. Nowadays spiral CT [34], [35] is becoming increasingly popular for cardiac imaging, with image quality rivaling that of magnetic resonance. DSR [18] uses multiple X-ray tubes and image intensifier chains to produce "real time" multiple cross sections with similar acquisition times to ultrafast CT but is not commercially available [15]. EBCT [36] or Ultrafast CT is both relatively inexpensive to perform and capable of providing 3-D information on coronary calcium deposits (plaque) and cardiac cavities' anatomy and function. A current limitation of this system (relative to DSR) is that the spatial resolution in the transaxial direction is much less than in the in-plane (often transverse) direction.

E. MRI

Cardiac MRI [21] is now an established, although still rapidly advancing, technique providing information on morphology and function of the cardiovascular system [37]. Advantages of cardiac MRI include a wide topographical field of view with visualization of the heart and its internal morphology and surrounding mediastinal structures, the capability of multiple imaging planes, and a high soft-tissue contrast discrimination between the flowing blood and myocardium without the need for contrast medium or invasive techniques. Long- and short-axis views of the heart, as used in echocardiography, can be obtained routinely since arbitrary imaging planes can be selected.

Another advantage of MRI is that it can provide both anatomical and functional information about the heart. Several researchers have used MRI to assess global and regional, RV and LV function as represented by SV, EF and LV mass [38]–[43], wall-thickening [44], myocardial motion [45], and circumferential shortening of myocardial fibers [46]. Data from MRI is more accurate than that derived from LV angiocardiography, where the calculation is based on the assumption that the LV is ellipsoidal in shape. Volume measurements by MRI are independent of cavity shape, with the area from contiguous slices integrated over the chamber of interest.

In contrast with other techniques, including 2DE and angiocardiography, anatomic information is easily defined on MRI. The advantages of MRI over 2DE are a wider topographical window and a superior contrast resolution.

A decade ago, MR *tagging* was introduced independently by Zerhouni [47] and Axel [48]. This technique is able to create and track material points (points attached to a fixed location of the

TABLE II
OVERVIEW OF CARDIAC MODELING METHODS: REPORTED CLASSICAL FUNCTIONAL PARAMETERS AND THEIR VALIDATION. SEE KEYS AND NOTES IN FIG. 4

Evaluation	Reference	Modality	Parameters		Flexibility	Pre-processing	Automation	*Ad hoc*	Validation/Illustration		
			Global	Motion	Complexity				Type	No.	Std. of Ref.
Qualitative or No evaluation	Amini [86]	DSR,MR	–	*MF*	L	M	+	+	a	1	*NA*
	Bartels [144,184]	NS	–	*MF*	L	N	+	+	m	1	GT
	Benayoun [90]	DSR	–	*MF*	L	A	+	–	a	1	*NA*
	Cauvin [103]	SPECT	*LVV*	–	C	A	+	–	P	*NA*	*NA*
	Chen [107]	BA	*LVV*	*SA*	H	M	–	–	V	1	*NA*
	Chen [109]	DSR	*LVV*	–	C	N	+	–	V	1	*NA*
	Gustavsson [105]	US	*LVV*	–	H	M	=	+	V	1	*NA*
	Huang [120]	DSR	*LVV*	*MF*	L	M	+	+	a	1	*NA*
	Kerwin [74]	MR^{tag}	–	*SA*	L	A†	+	–	V	1	*NA*
	Matheny [111]	DSR	*LVV*	–	G	M	+	–	a	1	*NA*
	Maehle [29]	US	*LVV*	*WT*	L	M	–	–	V/P	*NA*	*NA*
	McInerney [124]	DSR	*LVV*	*MF*	L	I	–	–	V	1	*NA*
	Niessen [136]	MR/DSR	*LVV*	*WT*	L	I	+	+	a	1/1	*NA*
	O'Donnell [7,8]	MR^{tag}	*LVV*	*WT,SA*	H	M	+	+	V	1	*NA*
	Papademetris [152]	US	–	*SA*	L	A	+	–	a	3	*NA*
	Pentland [102]	X	*LVV*	*MF*	G	I	+	+	V	1	*NA*
	Radeva [147]	MR^{tag}	*LVV*	*MF,SA*	L	M	–	+	V	1	*NA*
	Rueckert [128]	MR	*LVV*	*MF*	L	I	+	+	V	1	*NA*
	Staib [112]	DSR/MR	*LVV*	–	G	I	+	+	a	1/1	*NA*
	Yezzi [133,134]	MR	*LVV*	*WT*	L	I	+	+	V	1	*NA*
	Young [60,100]	BA	–	*SA*	L	M	+	+	a	1	*NA*
	Young [148]	MR^{tag}	–	*SA*	L	I	–	+	V	1	*NA*
Quantitative: synthetic, phantom and animal models	Bardinet [113]	DSR	**LVV**	*MF*	H	M	+	–	a/m	1	OB/AS
	Czegledy [104]^{RV}	CT	**RVV**	–	C	M	=	–	p	10	AT
	Denney [73,191]	MR^{tag}	–	**MF**	L	A†	+	–	m/a	1/1	GT/*NA*
	Denslow [108]^{RV}	MR	**RVV**	–	C	M	=	–	p	13	AT
	Germano [33,122,123,163]	SPECT	**LVV,EF**	–	H	A	+	–	p	1	GT
	Gopal [25]	US	**LVV**	–	L	M	+	–	p	17	AT
	Kerwin [74]	MR^{tag}	–	*SA*‡	L	A†	+	–	m	–	GT
	Haber [140,141]^{RV}	MR^{tag}	–	**MF**,*SA*	L	M	+	+	m	1	GT
	Huang [149]	MR^{tag}	–	**MF**,*SA*	L	A	+	–	m/a	–/1	GT/*NA*
	Legget [26,192,193]	US	**LVV,LVM**	–	L	M	=	–	p/a	6/21+5	GT/AT
	Moore [69]	MR^{tag}	–	**SA**	L	A†	+	–	m	–	AS
	Moulton [146]	MR^{tag}	–	**SA**	L	M†	+	–	m/a	–/7	NS/NS
	O'Dell [145]	MR^{tag}	–	**SA**	H	M†	+	–	m	–	AS
	Papademetris [150,151]	MR	–	**SA**	L	A	+	–	a/a	8/3	AT
	Sacks [106]^{RV}	MR	–	**WT**	L	M	=	+	p/a	6/1	GT/*NA*
	Sato [115]	BA	**LVV**	–	L	M	–	+	m/p	1/1	GT/AT
	Spinale [101]^{RV}	BA	**RVV,SV**	**WT**	L	M	=	+	p/a	22/24	AT/AT
	Shi [129]	MR/DSR	–	**WT,MF**	L	A	+	+	a	12	AT
	Shi [142]	MR	–	*MF*,**SA**	L	A	+	-	a	1	CL
	Tu [126]	DSR	**LVV**	–	G	M	+	+	a	2	OB
	Yettram [98,99]	BA	**LVV**	–	L	M	=	–	p	8	AT
	Young [68]	MR^{tag}	–	**SA**	L	M	+	–	m	–	AS
Quantitative: clinical case studies without standard of reference	Declerck [114]	SPECT	–	**MF**	G	A	+	+	V/P	3/1	*NA*
	Kuwahara [143,194]	BA	**LVV,EF,SV**	–	L	M	=	–	P	13	*NA*
	Legget [26,193]	US	**LVV**	–	L	M	–	–	V/P	6/2	*NA*
	Moore [69]	MR^{tag}	–	**SA**	L	A†	+	–	V	1	*NA*
	O'Dell [145]	MR^{tag}	–	*SA*‡	H	M†	+	–	V	10	*NA*
	Park [5]	MR^{tag}	*LVV*,**EF**	*MF*	C	M	+	+	V/P	1/1	*NA*
	Park [6]	MR^{tag}	*LVV*	**MF**,*SA*	C	M	+	+	V/P	1/1	*NA*
	Young [60,100]	BA	–	**SA**	L	M	+	+	V	1	*NA*
	Young [68]	MR^{tag}	–	**SA**	L	M	+	–	V	1	*NA*
Quantitative: clinical case studies with standard of reference	Bardinet [113]	SPECT	**LVV**	*WT,MF*	H	M	+	–	V	1	OB
	Biedenstein [132]	SPECT	**LVV**	–	L	I	+	–	P	42	OB
	Coppini [27]	US	**LVV,EF**	–	L	N	+	–	V	3	OB
	Faber [118]	SPECT/MR	**LVV**	*WT*	L	I	+	+	V/P	22/16	OB
	Faber [121]	SPECT	**LVV**	–	L	I	+	+	P	10	OB(m)
	Germano [33,122,123,195]	SPECT	**LVV,EF**	**WT**	H	A	+	–	P	144/65	OB(m)/AT
	Geiser [116,117]	US	*LVV*,**EF,SV,CO**	*WT*	L	M	=	–	P	4	AT
	Goshtasby [110]	MR	**LVV**	–	L	I	+	+	V	5	OB
	Legget [26,192]	US	**LVV,SV**	–	L	M	–	–	V	5	AT
	Ranganath [125]	MR	**LVV,EF**	–	L	I	+	+	V	7	OB
	Tseng [179]	US	**LVV**	**WT**	G	I	=	–	V	1	OB

myocardium) over time. Myocardial deformations can, therefore, be studied in a noninvasive manner. SPAMM creates two orthogonal sets of parallel planes (sheets) of magnetic saturation, usually orthogonal to the imaging plane. Tissue deformation will be indicated by the displacement of black (saturated) bands in the image that correspond to the intersections of the

Keys to Table II:

NA = not available / reported

Parameters: **bold** = quantitative results reported; *italic* = computable from the model (but quantitative results not reported). Motion parameters were classified in three categories: WT = wall thickening analysis, MF = wall/tissue motion field (not including strain analysis), SA = strain analysis.

Flexibility: C = compact model with small or medium number of degrees of freedom (DOF), G = flexible model with global support basis function and large number of DOF, L = flexible model with local support basis functions and large number of DOF, H = hierarchical models.

Pre-processing to initialize the model. N = none; M = manual segmentation of contours and/or land-marks; A = (semi) automatic delineation of contours and/or land-marks; I = approximated model initialization or land-mark placement. Pre-computation of feature images (gradient, Laplacian, etc.) was not considered as pre-processing.

Automation after pre-processing and selection of *ad hoc* parameters: (+) full, (−) interactive guidance may be required to correct/assist intermediate steps, (=) relying on substantial human guidance.

Ad hoc parameters: (−) none, or robustness demonstrated through sensitivity analysis, (+) yes and no sensitivity analysis was performed.

Validation/Illustration information. *Type* of evaluation/illustration set: m = mathematical models, p = physical phantoms (mostly balloons or heart casts), a = animal model, V = human volunteers and P = patients.

Standard of reference: AS = analytic solution, AT = alternative technique, CL = comparison to literature, GT = ground truth, NS = numerical solution, OB(m) = human observer (involving multiple modalities). Papers with several evaluation studies have multiple entries.

Notes:

‡Only the accuracy in determining tag intersections was computed. No quantitative analysis reported on deformation field or strain analysis.

†Monte Carlo analysis of sensitivity for this factor is reported.

Fig. 4. Keys and notes to Table II.

imaging plane (tag grid). This grid only provides the in-plane motion component (2-D motion). To reconstruct the 3-D motion of the material points, a number of 2-D tagged image sections must be obtained in at least two orientations. Further postprocessing is then required to interpolate the displacement field and to eventually perform strain analysis.

III. Classical Descriptors of Cardiac Function

Development of models of the cardiac chambers has emerged from different disciplines and with various goals. Cardiac models have been used for deriving functional information, for visualization and animation, for simulation and planning of surgical interventions, and for mesh generation for FE analysis.

This survey will be confined to the application of modeling techniques for obtaining classical functional analysis. Classical functional analysis can be divided into *global functional analysis* (Section III-A), and *motion/deformation analysis* (Section III-B), from which the most clinically relevant parameters can be obtained.

Model-based methods also allow one to derive new descriptors of cardiac shape and motion. Such advanced descriptors have been mainly presented in the technical literature and their clinical relevance has still to be assessed. Without pretending to be exhaustive, Appendix A summarizes a number of nonclassical shape and motion descriptors that demonstrate the extra possibilities provided by some advanced methods.

A. Global Functional Analysis

Weber and Hawthorne [49] proposed a classification of cardiac indexes according to their intrinsic dimensionality: linear, surface and volumetric descriptors. Linear parameters have been used intensively in the past since they can easily be derived from 2-D imaging techniques like 2DE and X-ray angiocardiography.[4] However, they assume an "idealized" geometry of the LV and strongly depend on external or internal reference and coordinate systems. Besides total ventricular wall area, other surface indexes based on curvature and derived parameters have been investigated from 2-D studies [50]–[53]. More recently, many image processing approaches to LV modeling have suggested true 3-D global and local shape indexes based on surface properties.

In practice, assessment of cardiac function still relies on simple global volumetric measures like LVV and mass, and EF. These and other basic parameters will be presented in the following paragraphs.

Left Ventricular Volume (LVV): is a basic parameter required to derive other LV indexes like, e.g., EF. Angiocardiography and echocardiography have been traditionally used to assess this quantity. In the latter case, three approaches have been applied: represent the LV volume 1) as the volume of a single shape (e.g., truncated ellipse); 2) as the sum of multiple smaller volumes of similar configuration (e.g., Simpson's method), and 3) as a combination of different figures [14, p. 585]. The achieved accuracy in the assessment of LVV with echocardiography varies largely with the model used to represent the LV. The best results have been obtained using Simpson's rule where *in vitro* studies have revealed a relative error ranging from 5.9% to 26.6% depending on the particular implementation and the number of short-axis slices used in the computation [14, p. 588]. It has been shown that echocardiography consistently underestimates ventricular cavity, while angiocardiography consistently overestimates true volumes [14]. In a recent study by Lorenz *et al.* [42] with a canine model and autopsy validation, it has been shown that cine MRI is a suitable and accurate method to estimate RVV and LVV. In this study, MR-based and autopsy volumes agreed within 6 ml, yielding no statistically significant differences.

Left Ventricular Volume (LVM): LV hypertrophy, as defined by echocardiography, is a predictor of cardiovascular risk and higher mortality [14, p. 599 and references therein]. Anatomically, LV hypertrophy is characterized by an increase in muscle mass or weight.

LVM is mainly determined by two factors: chamber volume, and wall thickness. There are two main assumptions in the computation of LVM: 1) the interventricular septum is assumed to be part of the LV and 2) the volume, V_m, of the myocardium is equal to the total volume contained within the epicardial borders of the ventricle, $V_t(\mathrm{epi})$, minus the chamber volume, $V_c(\mathrm{endo})$;

[4]Such parameters are, for instance, left ventricular internal dimension (LVID), relative wall thickness (RWT), and estimates of fractional shortening of the cardiac fibers ($\%\Delta D$) and their velocity (V_{cf}). For a detailed analysis of these parameters the reader is referred to Vuille and Weyman [14].

LVM is obtained by multiplying V_m by the density of the muscle tissue (1.05 g/cm^3)

$$V_m = V_t(\text{epi}) - V_c(\text{endo}) \quad (1)$$

$$\text{LVM} = 1.05 \times V_m. \quad (2)$$

LVM is usually normalized to total body surface area or weight in order to facilitate interpatient comparisons. Normal values of LVM normalized to body weight are 2.4 ± 0.3 g/kg [42].

Stroke Volume (SV): is defined as the volume ejected between the end of diastole and the end of systole.

$$\text{SV} = \text{end-diastolic volume (EDV)} - \text{end-systolic volume (ESV)} \quad (3)$$

Alternatively, SV can be computed from velocity-encoded MR images of the aortic arch by integrating the flow over a complete cardiac cycle [54]. Similar to LVM and LVV, SV can be normalized to total body surface. This corrected SV is known as SVI. Healthy subjects have a normal SVI of 45 ± 8 ml/m^2 [42].

Ejection Fraction (EF): is a global index of LV fiber shortening and is generally considered as one of the most meaningful measures of the LV pump function. It is defined as the ratio of the SV to the EDV

$$\text{EF} = \frac{\text{SV}}{\text{EDV}} \times 100\% = \frac{\text{EDV} - \text{ESV}}{\text{EDV}} \times 100\%. \quad (4)$$

Lorenz *et al*. measured normal values of EF with MR [42]. They found values of $67 \pm 5\%$ (57%–78%) for the LV, and $61 \pm 7\%$ (47%–76%) for the RV. Similar values were obtained with ultrafast CT, echocardiography, and X-ray angiocardiography [14], [42].

Cardiac Output (CO): The role of the heart is to deliver an adequate quantity of oxygenated blood to the body. This blood flow is known as the *cardiac output* and is expressed in liters per minute. Since the magnitude of CO is proportional to body surface, one person may be compared to another by means of the CI, that is, the CO adjusted for body surface area. Lorenz *et al.* [42] reported normal CI values of 2.9 ± 0.6 l/min/m^2 and a range of 1.74–4.03 l/min/m^2.

CO was originally assessed using Fick's method or the indicator dilution technique [55]. It is also possible to estimate this parameter as the product of the volume of blood ejected within each heart beat (the SV) and the HR.

$$\text{CO} = \text{SV} \times \text{HR} \quad (5)$$

In patients with mitral or aortic regurgitation, a portion of the blood ejected from the LV regurgitates into the left atrium or ventricle and does not enter the systemic circulation. In these patients, the CO computed with angiocardiography exceeds the forward output. In patients with extensive wall motion abnormalities or misshapen ventricles, the determination of SV from angiocardiographic views can be erroneous. Three-dimensional imaging techniques provide a potential solution to this problem since they allow accurate estimation of the irregular LV shape.

B. Motion and Deformation Analysis

Motion analysis[5]*:* A number of techniques have been used in order to describe and quantify the motion of the heart. They can be divided into three main categories [56]: i) detecting endocardial motion by observing image intensity changes, ii) determining the boundary wall of the ventricle, and subsequently tracking it, and iii) attempting to track anatomical [57]–[60], implanted [61]–[67] or induced [47], [48], [68]–[74] myocardial landmarks. There are a few problems involved with each of these techniques. Assumptions must be made about the motion (motion model) in the first two groups in order to obtain a unique point-wise correspondence between frames. To this end, optic flow methods [75]–[80][6] and phase contrast MR [82]–[85] have been applied for i), and curvature-based matching [86]–[90] has been used to find point correspondences in ii). Landmark-based methods [47], [48], [57]–[74] provide information on material point correspondence. However, this information is mostly sparse and, again, assumptions on the type of motion have to be made in order to regularize the problem of finding a dense displacement field. The use of implanted markers adds the extra complication of being invasive, which precludes routine use of this technique in humans. Although implanted markers are usually regarded as the gold standard, there are some concerns in the literature about their influence on both image quality and modification of the motion patterns.

Wall Thickening (WT): Azhari *et al.* [91] have compared WT and wall motion in the detection of dysfunctional myocardium. From their study, it was concluded that WT is a more sensitive indicator of dysfunctional contraction [91]. This finding has triggered several researchers to define methods to quantify wall thickness. Azhari *et al.* [91], and Taratorin and Sideman [92] carried out a regional analysis of wall thickness by dividing the myocardium into small cuboid elements. The local wall thickness is then defined as the ratio between the volume of the particular element and the average area of its endocardial and epicardial surfaces [44].

The most widely employed method for WT computation, however, is the *centerline method* [93] and several improvements thereof [41], [94]–[96]. Starting with the endocardial and epicardial contours at each slice, the centerline method, in its original formulation, measures WT in chords drawn perpendicular to a line that is equidistant to both contours (the centerline). Although more accurate than methods relying on a fixed coordinate system, this method still assumes that the contours are perpendicular to the long axis of the LV. If this is not the case, the myocardial wall thickness is overestimated which invariably occurs, for instance, in slices that are close to the apex. Buller and co-workers [41], [94] introduced an improvement on this method by estimating at each location the angle between the wall and the imaging plane. Recently,

[5]At this point it is worth mentioning an excellent on-line bibliographic database maintained by the Special Interest Group on Cardiac Motion Analysis (SigCMA) that can be accessed at http://www-creatis.insa-lyon.fr/sigcma. It also provides general bibliographic information on model-based cardiac image analysis.

[6]For a survey of optic flow methods in computer vision, see Beauchemin and Barron [81].

Bolson and Sheehan [95], [96] have introduced the *center-surface method* (true 3-D extension of the centerline method) which makes use of a reference medial surface to compute the chords and subsequent wall thickness.

Strain Analysis (SA): is a method to describe the internal deformation of a continuum body. It is an appealing tool to study and quantify myocardial deformation. Here, we shall briefly introduce some of the concepts related to SA. A comprehensive exposition of this theory can be found in Fung [97].

To describe the deformation of a body the position of any point in the body needs to be known with respect to an initial configuration; this is called the *reference state*. Moreover, to describe position a *reference frame* is needed. In the following a Cartesian reference frame will be assumed. It is also common to use curvilinear coordinates for which some of the expressions simplify.

A myocardial point, $\mathbf{M}_r$, has coordinates $\{y_i\}$ and a neighboring point, $\mathbf{M}'_r$, has coordinates $\{y_i+dy_i\}$. Let $\mathbf{M}_r$ be moved to the coordinates $\{x_i\}$, and its neighbor to $\{x_i+dx_i\}$. The deformation of the body is known completely if we know the relationship

$$x_i = x_i(y_1, y_2, y_3) \quad i = 1, 2, 3 \tag{6}$$

or its inverse

$$y_i = y_i(x_1, x_2, x_3) \quad i = 1, 2, 3. \tag{7}$$

For every point in the body we can write

$$x_i = y_i + u_i \quad i = 1, 2, 3 \tag{8}$$

where u_i is called the *displacement* of the particle $\mathbf{M}_r$. In order to characterize the deformation of a neighborhood, the first partial derivatives of (6)–(8) are computed. These derivatives can be arranged in matrix form to define the *deformation gradient tensor*: $F = [\partial x_i/\partial y_j]$, $(i, j = 1, 2, 3)$. The deformation gradient tensor enables to estimate the change in length between the neighboring points $\{y_i\}$ and $\{y_i + dy_i\}$, when they are deformed into $\{x_i\}$ and $\{x_i+dx_i\}$. Let $d\ell_r$ and $d\ell$ be these lengths before and after deformation. Then

$$d\ell^2 - d\ell_r^2 = 2\sum_{i=1}^{3}\sum_{j=1}^{3} E_{ij}\, dy_i\, dy_j \tag{9}$$

where $E = [E_{ij}]$ is the *Green strain tensor* [97]

$$\begin{aligned} E_{ij} &= \frac{1}{2}\left(\sum_{k=1}^{3}\frac{\partial x_k}{\partial y_i}\frac{\partial x_k}{\partial y_j} - \delta_{ij}\right) \\ &= \frac{1}{2}\left(\frac{\partial u_i}{\partial y_j} + \frac{\partial u_j}{\partial y_i} - \sum_{k=1}^{3}\frac{\partial u_k}{\partial y_i}\frac{\partial u_k}{\partial y_j}\right) \end{aligned} \tag{10}$$

where δ_{ij} is the Kronecker tensor. From the strain tensor it is possible to decompose the strains into two groups: *axial* and *shear* strains. The former correspond to the diagonal elements and represent changes in length aligned with the axes of the reference frame while the latter correspond to off-diagonal terms or deformations where two axes are coupled.

IV. Overview of Modeling Techniques

A large effort has been devoted to the analysis and segmentation of cardiac images by methods guided by prior geometric knowledge. When focusing on the way models are geometrically represented, three main categories can be distinguished: *1)* surface models, *2)* volumetric models, and *3)* deformation models. In all cases both discrete and continuous models have been proposed as well as implicitly defined surface models (Fig. 2).

Alternatively, one may classify model-based approaches by considering the information that is used as input for model recovery. This categorization is highly determined by the imaging modality for which the method has been developed. There are a variety of inputs for model recovery: *1)* multiple 2-D projection images, *2)* multiple oriented 2-D slices, *3)* fully 3-D grey-level images, *4)* 3-D point sets, *5)* phase-contrast velocity fields, and *6)* MR tagging information.

In this survey we will compare the different methods with respect to type of model representation, and types of input data and features that the model is recovered from. Table I, in which the different approaches are grouped according to the type of model representation, summarizes this section.

A. Surface Models

Many approaches to cardiac modeling focus on the endocardial (and/or epicardial) wall. Three subcategories are proposed: 1) continuous models with either global, local, or hybrid parameterizations, 2) discrete models, and 3) implicitly defined deformable models.

1) Continuous Models: In the early studies of cardiac images by 2DE and angiocardiography, cardiologists used simplified models of the LV in order to compute functional parameters like ventricular volume and mass from 2-D images. Most of the times, simple ellipsoidal models were considered. See, e.g., Vuille and Weyman [14] and Dulce *et al.* [40] for a comprehensive review of such models and a comparison of their accuracy. In the last decades, however, approaches have appeared that make use of 3-D acquisitions to reconstruct models varying from global parameterizations of the LV surface [5], [27], [103], [110]–[112], [114], [153] to hierarchically parameterized models [9], [105], [107], [123], [137].

Global approaches: In this category, we will discuss surface representations that are based on simple geometric models. In general they can provide, with a limited number of global parameters, a rough shape approximation. We also include in this category surface representations obtained as series of basis functions with global support.

Cauvin *et al.* [103] model the LV as a *truncated bullet*, a combination of an ellipsoid and a cylinder, that is fitted to the morphological skeleton of the LV. Metaxas and Terzopoulos [154] have proposed *superquadrics* [155] to model simple objects with a small number of parameters. Since the introduction of superquadrics, several extensions have appeared in the literature. Chen *et al.* [109] apply superquadrics with tapering and bending deformations to model the LV in an integrated approach for image segmentation and shape analysis. The method iterates

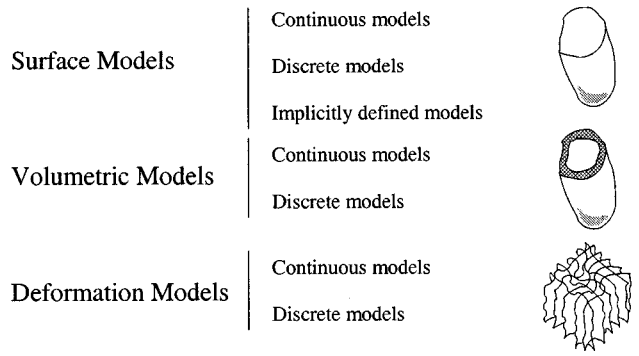

Fig. 2. Proposed classification of cardiac modeling approaches.

between a region-based clusterization step [156], using statistics of image intensity and gradient, and a shape-based step that checks the consistency between the current segmentation and a superquadric model. Park, Metaxas and Axel [6] have extended the flexibility of superquadrics by introducing *parameter functions*: radial and longitudinal contraction, twisting and long-axis deformation. These allow for a more detailed representation of the LV while keeping the intrinsic geometrical meaning of the superquadric parameters. LV mid-wall motion is recovered using preprocessed MR tagging data obtained by sampling the LV mid-wall surface from the 3-D FE model of Young and Axel [68].

Staib and Duncan [112] use *sinusoidal basis* functions to decompose the endocardial surface of the LV. The overall smoothness of the surface is controlled by decreasing the number of harmonics in the Fourier expansion. Model recovery is cast into a Bayesian framework in which prior statistics of the Fourier coefficients are used to further limit the flexibility of the model. Matheny and Goldgof [111] compare different 3-D and four-dimensional (4-D) surface *harmonic descriptions* for shape recovery. Time can be incorporated in two ways in the model: 1) hyper spherical harmonics, where an event in space-time is converted from Cartesian coordinates to hyper spherical coordinates and 2) "time-normal" coordinates which are formed by including a temporal dependency to each spatial coordinate. Experiments carried out with a 3-D CT data set of a canine heart have indicated that hyper spherical harmonics can represent the beating LV with higher accuracy than direct normal extensions of spherical, prolate spheroidal and oblate spheroidal harmonics. Coppini *et al.* [27] reconstruct a 3-D model of the LV based on apical views in US images. LV boundaries are obtained by grouping edges with a feed-forward NN integrating information about several edge features (position, orientation, strength, length, and acquisition angle). This allows discarding many edge points that are not plausible LV boundary points. The 3-D LV geometry is modeled as a spherical elastic surface under the action of radial springs (attracting the model to the edge points); a Hopfield [157] NN is used to solve the minimization problem involved in the reconstruction of this surface. Declerck *et al.*[114] have introduced a spatio-temporal model to segment the LV and to analyze motion from gated-SPECT sequences. The model relies on a *planispheric transformation* that maps endocardial points in one time frame to the corresponding material points in any other frame. First, endocardial edge points are detected in all frames using a Canny-Deriche edge detector [158] in spherical coordinates [159]. Selected points in subsequent frames are matched to the current frame using a modification of the ICP algorithm [159]–[161]. Based on corresponding point pairs, the parameters of a planispheric transformation are retrieved by least-squares approximation. This transformation allows to describe motion with just a few parameters and to relate them to a canonical decomposition (radial motion, twisting motion around the apico-basal axis, and long-axis shortening).

Hierarchical approaches: Some authors have addressed the problem of building hierarchical representations where a model described with few parameters is complemented with extra deformations that capture finer details. Gustavsson *et al.* [105], for instance, employ a *truncated ellipsoid* to obtain a coarse positioning of the LV cavity from contours drawn in two short-axis and three apical echocardiographic views. Further model refinement is achieved using cubic B-spline curves approximating manually segmented contours in multiple views. Chen *et al.* [107] and Bardinet *et al.* [9] use superquadrics [155] to coarsely describe the LV. Their approaches fundamentally differ in the representation of the additional deformation field. Chen *et al.* use spherical harmonics in order to approximate the residual error between the superquadric estimate of the endocardial LV wall and the true wall location. Spherical harmonics have the advantage that fine-tuning can be improved *ad infinitum* with increasing number of harmonics. However, adding a new coefficient influences the shape of the model everywhere (nonlocal basis functions). Bardinet *et al.* [9] extend the basic superquadric deformations (tapering and bending) through the use of FFDs, a technique introduced in computer graphics by Sederberg and Parry [162]. The superquadric is attached to a flexible, box-like frame, inducing a nonrigid deformation on the superquadric. Bardinet *et al.*use trivariate B-splines to parameterize this deformation field. In a later work, Bardinet *et al.* [113] apply their method to estimate LV wall motion. This is accomplished by deforming the full model (superquadric+FFD) in the first frame, and modifying only the FFD in the subsequent frames. By tracking points with the same parametric coordinates along the cardiac cycle, a number of dynamic parameters like WT and twisting motion are computed. Germano *et al.* [122], [123] have developed a system for automatic quantification of LV function from gated-perfusion SPECT images. An iterative algorithm fits an ellipsoidal model to a semiautomatically obtained segmentation. This iterative algorithm incrementally adapts the ellipsoid's parameters and center of mass so that accurate registration of the model is obtained even in the presence of large perfusion defects. The ellipsoid defines a coordinate system that is used to refine the model. A Gaussian model of the count profiles is used to compute radial offsets corresponding to the endocardial and epicardial walls. Although simple in its formulation, this method has proven very useful in determining most of the classical cardiac functional parameters [33] from SPECT images and has been extensively validated in humans [122], [123], [163].

Local approaches: A number of methods have been reported to provide surface reconstruction using piecewise

polynomial surfaces, e.g., B-splines or bicubic Hermite surface patches. These techniques have appeared mainly in the context of surface reconstruction from multiple cross sections [29], [143] or projections [98]–[101], [115]. Given the ill-posed nature of this problem, most of these techniques require extensive user interaction. Usually, a set of landmarks or fiducial points are determined from each cross section/projection and, using high-level knowledge about the viewpoint and the geometry of the LV, a local surface approximation using surface patches is performed.

A rather different approach is the one by Pentland and Horowitz [102] who applied modal analysis and FE to reconstruct a 3-D model of the LV from X-ray transmission data. Modal analysis offers a principled physically based strategy for reducing the number of DOFs of the model and to obtain an over-constrained problem for shape recovery. Optic flow is used to derive the deformation of the 3-D model from the 2-D views, and a Kalman filter for tracking the structures over time.

Instead of working with multiple cross sections or projection images, Goshtasby and Turner [110] segment LV and RV endocardial surfaces from 3-D flow-enhanced MR images. In this case, the endocardial surface is modeled as a deformable cylinder using rational Gaussian surfaces [164]. The model is deformed to fit the zero-crossings of the image Laplacian. To avoid attraction by spurious edges, prior to fitting, the feature map is masked by a rough LV region-of-interest obtained by intensity thresholding.

RV models: Some efforts have also been directed toward geometric modeling of the RV. This chamber has a more complex shape than the LV. Spinale *et al.* [101] fit semiellipses to model the crescentic shape of the RV from biplane ventriculograms. Czegledy and Katz [104] model the RV using a crescentic cross-sectional model composed of two intersecting circles of different radii. This 3-D model is parameterized by only a few linear dimensions that can be measured directly from CT, MR, or US images. From these dimensions, the RVV is approximated using analytical expressions. Denslow [108] model the RV as the difference of two ellipsoids (an ellipsoidal shell model). The parameters from this shell are estimated from MR images (a long-axis and a four-chamber view) and from those, volume estimates can be derived. Sacks *et al.* [106] model the endocardial and epicardial walls of the RV by biquadric surface patches (contours were manually traced from MR images), and have studied surface curvature and wall thickness changes along the cardiac cycle using this representation.

2) Discrete Models: An alternative to continuous surface representations is the use of discrete surface models. Several methods have been reported in the literature and they can be grouped in the following way.

Physics-based models: Physics-based modeling has attracted the attention of many computer vision researchers. In this framework, surface recovery is cast into the deformation of a virtual body (the geometric model plus its material properties) under virtual external forces derived from image/point features, or user-defined constraints. In the final (deformed) state, this virtual body reaches an equilibrium between the external forces and internal (regularization) constraints. A good overview of the theory of physics-based deformable models and its applications can be found in the book by Metaxas [165] and in the survey by McInerney and Terzopoulos [3].

McInerney and Terzopoulos [124] have applied this theory to the segmentation and tracking of the LV in DSR image sequences. A FE balloon [166] deformable model is discretized using triangular elements, and deformed according to a first-order approximation of the Lagrange equations of motion. User-defined point constraints can be interactively inserted to guide the deformation of the model and to avoid local minima of the potential energy in which the model is embedded. In the Lagrangian formulation, 3-D image sequences can easily be handled by making the potential energy a function of time. Montagnat, Delingette and Malandain [131] apply simplex meshes [167] to reconstruct the LV from multiple views of a rotating US probe. Images are acquired in cylindrical coordinates coaxial with the apico-basal axis. Accordingly, images are filtered in cylindrical coordinates. Boundary points are detected based on a combination of image gradient and intensity profiles normal to the surface. Finally, detected edge points are cast into point attraction-forces deforming the model according to Newton's law of motion. Ranganath [125] reconstructs 3-D models of the LV from MRI images using multiple 2-D *snakes* [168] and devising efficient mechanisms for interslice and interframe contour propagation. Biedenstein *et al.* [132] have recently published an elastic surface model and applied it to SPECT studies. The elastic surface is deformed according to a second-order partial differential equation. The external (image) forces are derived from the radioactive distribution function and push the elastic surface toward the center surface of the LV wall. Wall thickness can be then computed as the distance between the elastic surface and the mass points of the radioactivity distribution gradient. Huang and Goldgof [120] have presented an adaptive-size mesh model within a physics-based framework for shape recovery and motion tracking. The optimum mesh size is inferred from image data, growing new nodes as the surface undergoes stretching or bending, or destroying old nodes as the surface contracts or becomes less curved. The method is employed to analyze LV motion from a DSR dataset. To establish point correspondences, an adaptive-size mesh is generated for the first frame to be analyzed; subsequent frames further deform this mesh while keeping its configuration fixed.

Physics-based modeling frequently makes an assumption that can be problematic: internal constraints are usually represented in the form of *controlled-continuity stabilizers* [169]. It is known that, in the absence of image forces, deformable models tend to shrink. To avoid this, Rueckert and Burger [128] simultaneously model the two cardiac chambers (RV and LV) using a GDT. The standard stabilizers on the deformed model are replaced by a stabilizer on the deformation field between a rest model and a deformed model. A GDT consists of three parts: 1) a set of vertices that defines the rest state (the template), 2) a set of vertices that defines a deformed state (an instance of the template), and 3) a penalty function that measures the amount of deformation of the template with respect to its equilibrium shape (the stabilizer). Another solution to the above mentioned problem, was proposed by Nastar and Ayache [127] who model a surface as a quadrilateral or triangular mesh of virtual masses. Each mass is attached to its neighbors by perfect identical springs with pre-

defined stiffness and natural length. The system deforms under the laws of dynamics. In addition to elastic and image forces, an "equilibrium force" determines the configuration of the mesh in the absence of external forces.

Spatio-temporal models: Several researchers have developed models that explicitly incorporate spatial *and* temporal variations of LV shape. Faber *et al.* [118] use a discrete 4-D model to segment the LV fom SPECT and MR images through a *relaxation labeling* scheme [170]. Endocardial and epicardial surfaces are modeled as a discrete template defined in a mixed spherical/cylindrical coordinate system co-axial with the LV long-axis. Each point in the template represents a radius connected to this axis. The model is spatio-temporal since the compatibility functions computed in the relaxation labeling scheme involve neighboring points both in space and time. In this way, surface smoothness and temporal coherence of motion are taken into account. Tu *et al.* [126] have proposed a 4-D model-based LV boundary detector for 3-D CT cardiac sequences. The method first applies a spatio-temporal gradient operator in spherical coordinates with a manually selected origin close to the center of the LV. This operator is only sensitive to moving edges, and less sensitive to noise compared to a static edge detector. An iterative model-based algorithm refines the boundaries by discarding edge points that are far away from the global model. The model is parameterized by spherical harmonics including higher order terms as the refinement proceeds.

Polyhedral models: LV polyhedral representations have been applied by several authors [25], [26], [116], [119], [121], [129]–[131] in the literature. The approaches differ either in the type of polygonal primitive (e.g., triangular or quadrilateral meshes) or the details of the shape recovery algorithm (imaging modality, input data or recovery features). Shi *et al.* [129], [130] use a Delaunay triangulation [171] to build a surface description from a stack of 2-D contours obtained with a combined gradient- and region-based algorithm [172]. This representation is subsequently used for motion analysis based on point correspondences. Bending energy under a local thin-plate model is used as a measure of match between models of consecutive frames. Friboulet, Magnin and Revel [119] have developed a polyhedral model to analyze the motion of the LV from 3-D MR image sequences. LV contours are manually outlined using a track-ball. After applying morphological and linear filtering to diminish quantization noise, the contours are radially resampled with constant angular step. Finally, the stack of resampled contours is fed into a triangulation procedure [173] which generates a polyhedral surface with approximately equal-sized triangles. Faber *et al.* [121] use a combination of cylindrical and spherical coordinate systems to build a discrete model of the LV in SPECT perfusion images. A radius function defined in a discrete (orientation) space of longitudinal and circumferential coordinates describes the LV. For each orientation, the radius is determined by finding the position of maximal perfusion (which is argued to occur in the center of the myocardium). After low-pass filtering to remove outlier radii, the radius function is mapped back to Cartesian space where the surface is represented using triangular or quadrilateral meshes. This approach shares some features of the work described in Faber *et al.* [118] but is purely static. Legget *et al.* [26], [174] use piecewise smooth subdivision surfaces [175] to reconstruct the LV geometry from manually traced contours in 3-D US images. Some elements of the mesh can be labeled so that they allow for sharp edges (e.g., at the mitral annulus and apex) and to define regional surface descriptors. Also, from 3-D US images, Gopal *et al.* [25] apply triangulated surfaces to reconstruct the geometry of latex balloons phantoms mimicking the LV. Three-dimensional reconstruction is directly obtained by triangulating the points of manually delineated contours from a stack of quasiparallel slices.

3) Implicitly Defined Deformable Models: Either in continuous or discrete form, the models in the two previous paragraphs were characterized by having an explicit surface parameterization. A surface model can also be defined by means of an implicit function. For instance, in the *level-set* approach, a model is obtained as the zero level set of a higher-dimensional embedding function. This technique, sometimes referred as *geodesic deformable models* have been introduced independently by Caselles *et al.* [176] and Malladi *et al.* [177] based on the work by Osher and Sethian [178]. Geodesic deformable models have been applied by Yezzi *et al.* [133], [134] to the segmentation of MR cardiac images. Recently, Niessen *et al.* [136] have extended the method to treat multiple-objects and have applied it to the segmentation of 3-D cardiac CT and MR images. Although geodesic models have the ability to handle changes in topology, unwanted and uncontrollable topological changes can occur in images of low-contrast edges or with boundary gaps since this is a purely data driven approach.

There are other types of implicit models not related to level-sets. Tseng *et al.* [179], for instance, use a NN to define a CDT to the LV boundary. A feed-forward NN is trained to learn the distance function to the endocardial and epicardial contours using a few hand-segmented image slices. The surface of the LV is then represented as the zeroes of the distance function. The NN can generalize the boundaries of the LV in the slices not included in the training set, thus serving as an aid to segment a 3-D image for which the user has to provide the segmentation of a few slices only. Under an affine deformation model, the distance transform is used to match different temporal frames and to derive motion parameters. Wall thickness is computed by the centerline method [93] using two CDT NNs for describing the endocardial and epicardial surfaces.

A third approach to implicit modeling is the use of surface primitives which are defined in implicit form. Lelieveldt *et al.* [137] segment thoracic 3-D MR images using hierarchical blending of hyperquadrics [180] and concepts of CSG [181]. The method provides an automatic, coarse segmentation of a multiple-object scene with little sensitivity to its initial placement. The most representative organs in the thorax (lungs, heart, liver, spleen, and cardiac ventricles) are incorporated in the model which can be hierarchically registered to the scanner coordinate system using only a few coronal, sagittal, and transversal survey slices. Owing to the contextual information present in the model, this sparse information has successfully been used to estimate the orientation of the long-axis of the LV. This allows an observer-independent planning of 3-D long-axis acquisitions in patients [182]. This technique was not designed to estimate accurate cardiac functional parameters but

can be used to generate a first initialization for more accurate algorithms.

B. Volumetric Models

As opposed to the plethora of surface representations, the use of volumetric models in the analysis and segmentation of cardiac images has received little attention.

O'Donnell *et al.* [7], [8] were the first to suggest a volumetric model to recover myocardial motion from MR tagging. The model, coined *hybrid volumetric ventriculoid*, can be decomposed into three parts: 1) a thick-walled superquadric, 2) a local offset either in nonparametric [7] or parametric [8] form, and 3) a local deformation in the form of a polyhedrization. The thick-walled superquadric represents a high-level abstraction model of the myocardium that is further refined by the local offsets. Altogether, these two parts constitute the rest model of the myocardium that is rigidly scaled to the dimensions of a new dataset. The local deformation field is responsible of capturing the detailed shape variability of different datasets. Park *et al.* [5] have extended their LV surface model [6] to a super-ellipsoid model with parameter functions. The model is fitted to tagged MR images providing a compact and comprehensive description of motion. Radial and longitudinal contraction, twisting, long-axis deformation, and global translation and rotation are readily available from the parameter functions. Alternatively, standard SA can be carried out. It is also possible to estimate other volumetric parameters like SV, CO, LVV, and LVM. In order to fit the model, a set of boundary points is manually delineated and a set of tags are semiautomatically tracked along the cardiac cycle using the algorithm of Young *et al.* [72]. Therefore, the accuracy of all volumetric measurements depends on the manual outlining.

Haber, Metaxas and Axel [140] have developed a model of biventricular geometry using FEs in a physics-based modeling context. The 3-D motion of the RV is analyzed by defining external forces derived from SPAMM MR tagging data [141]. Creswell *et al.* [138] and Pirolo *et al.* [139] describe a mathematical (biventricular) model of the heart built from 3-D MR scans of a canine specimen. Manual contour delineation of the epicardial, and LV and RV endocardial boundaries provides a set of points that is approximated with cubic nonuniform rational B-splines (NURBS [183]). From this representation, a hexahedral FE model is built in order to generate a realistic geometric model for biomechanical analysis.

Recently, Shi *et al.* [142] have introduced an integrated framework for volumetric motion analysis. This work extends the surface model of Shi *et al.* [129] by combining surface motion, extracted from MR magnitude images, and motion cues derived from MR phase contrast (velocity) images. The latter provide motion information inside the myocardial wall but are known to be less accurate at the boundaries [85]. The two sources of motion evidence (boundary and mid-wall motion) are fused by solving the discretized material constitutive law of the myocardium assuming a linear isotropic elastic material. In this framework, the measured boundary and mid-wall motion estimates at two consecutive frames are used as boundary and initial conditions of a FE element formulation. An advantage of this method with respect to physically-based techniques is that material properties can be set based on experimental knowledge about myocardial mechanical properties, and not on a virtual mechanical analog which usually leads to *ad hoc* parameter settings.

C. Deformation Models

Hitherto, we have focussed on representing either the endocardial (or epicardial) surface, or the volume comprised within the myocardial muscle. Tissue deformation, however, can be modeled without necessarily modeling the ventricular boundaries. To this end, material point correspondences in different temporal frames are required. These correspondences can be obtained by matching certain geometric properties over time (*general techniques*). If images are acquired using MR tagging technology, several other approaches can be applied that exploit the explicit correspondences inferible from tag displacements (*MR tagged-based techniques*).

1) General Techniques: Several techniques have been proposed in the literature for deformation recovery based on shape properties only. These methods are attractive because of their generality. On the other hand, one must reckon with the validity of the underlying assumptions and/or motion models before they are applied to analyze image sequences corresponding to normal and pathological myocardial motion patterns.

a) Continuous models: Amini and Duncan [86] have developed a surface model based on the assumption of *conformal* motion, where angles between curves are preserved but not distances between points. The LV surface is divided into locally quadric patches from which differential properties can be computed. Interframe patch correspondences are obtained using a metric that is minimal for conformal motion. An assumption of this model is that the subdivision into surface patches and the number of neighboring patches visited during the matching process are sufficient to accommodate for the largest stretching that can occur between frames. Bartels *et al.* [144], [184] model material deformations with multidimensional splines. The method shares properties of optical flow techniques to estimate motion fields. However, those approaches do not return an explicit model of the deformations (only displacements at discrete positions are provided). The main assumption of this technique is that, for a given material point, luminance is a conserved quantity. As in optic flow techniques, with only this assumption the solution remains under-constrained and, therefore, a regularization term must be added. Illustrations of the method on 2-D cardiac X-ray sequences are provided and the formulation readily extends to 3-D sequences. However, it is questionable whether luminance conservation can provide a reliable cue for deformation recovery in regions with homogeneous intensity, or in the presence of imaging artifacts and noise. For MR tagging, in particular, the approach must be adapted since luminance is not conserved due to the physics of the imaging process [75].

b) Discrete models: Benayoun and Ayache [90] propose an adaptive mesh model to estimate nonrigid motion in 3-D image sequences. The size of the mesh is locally adapted to the magnitude of the gradient, where the most relevant information is supposed to appear (e.g., cardiac walls). Mesh adaptation is carried out at the first frame only; subsequent frames

only deform the mesh to recover motion. The underlying hypothesis is that the deformation is small. Meshes at two time instants are registered through an energy-minimizing approach matching differential image properties (curvature and gradient). Recently, Papademetris *et al.* [150]–[152] have proposed a deformation model inspired by continuum mechanics. The method recovers a dense deformation field using point correspondences obtained with the point-tracking algorithm of Shi *et al.* [129]. Regularization is accomplished by measuring the internal energy of the myocardial tissue assuming a linear elastic body model. This is equivalent to a regularization term on the strain tensor space and not on the displacement field.[7] Anisotropy of the fibrous structure of the LV is accounted for in the internal energy by making the model stiffer in the fiber direction [185].

2) MR Tagging-Based Techniques: The introduction of MR tagging has stimulated researchers to develop models of cardiac tissue deformation. Compared to motion recovery based on point correspondences or optic flow, MR tagging has the advantage that, in principle, material point correspondences can be estimated from tag information. In this section, different approaches for modeling the deformation fields are reviewed. Accurate tag localization is a prerequisite for subsequent deformation recovery and, therefore, it is a closely related topic to deformation models. A brief overview of tag tracking techniques is given in Appendix B.

a) Continuous models: Several approaches have been proposed in which the parameterization of the deformation field is a continuous function. The availability of continuous deformation maps allows the computation of local strains. Young *et al.*, for instance, developed a model-based approach for tracking tag intersections [68] and tag stripes [72][8] that has been validated using silicone gel phantoms [188]. A deformation field that maps the first (undeformed) frame to a subsequent (deformed) frame is modeled through a piecewise polynomial function. Two fitting steps are involved in this method. First, the material points (tag intersections or stripes) in each deformed frame, $t > 0$, are reconstructed in the coordinate system of the undeformed state, $t = 0$ (*reconstruction fit*). In the latter frame, tag surfaces are arranged in true planes since no motion has occurred yet. In the second step, the material points for $t > 0$, expressed in the reference frame $(t = 0)$, are used to reconstruct a displacement field relative to $t = 0$ (*deformation fit*).[9]

[7]Related regularization schemes are the *global* and *body* smoothing terms described in Young and Axel [68] which act on the deformation gradient tensor. However, they are not directly interpretable as an internal deformation energy.

[8]Amini [186] have compared landmark-based (tag intersections) against curved-based tag (stripes) tracking based on the simulator of Waks [187]. It was concluded that as the number of stripes/landmarks increases, the two methods give similar performances. Under large deformations, the degradation of the curve-based techniques is more graceful compared to landmark-based methods.

[9]Both fitting steps handle sparse data and, therefore, regularization is needed. Regularization, however, is known to introduce artifactual strains. The effect of three regularization terms has been studied in [68]: 1) a *thin-plate spline* stabilizer, 2) a *global smoothing* regularizer minimizing the deformation gradient tensor, F, and 3) a *local body* regularizer minimizing the deformation gradient tensor expressed in some natural local coordinate system (e.g., aligned in circumferential, longitudinal and radial directions). Based on simulations of an axis-symmetric deformation of a thick walled incompressible cylinder, it was shown that all three constraints yield similar results in the SA.

A similar approach is followed by O'Dell *et al.* [145]. One-dimensional (1-D) displacements are obtained by three independent sets of tag lines: one in the cardiac long-axis, and two orthogonal sets in the short-axis view. Reconstruction of the deformation field is performed in two interpolation steps. The first step assumes a global affine transformation between two time frames. This is done to eliminate global bulk motion, and linear stretches and shear. In a second step, the residual deformation is interpolated using a prolate spheroidal decomposition to describe the curvilinear deformations expected in the heart.

Both Young *et al.* [68], [72] and O'Dell *et al.* [145] assume that the reference frame, to which the SA is related, is the undeformed state. This is normally the first frame in the sequence (planar tag surfaces). Although this simplifies the problem by allowing to decouple the motion component normal to the tagging plane, these methods cannot be used to compute strains between two arbitrary frames. The latter can be useful in order to retrospectively select the reference frame to coincide precisely with the diastole or systole, or to compute strains over a subset of the cardiac cycle. To circumvent this limitation, Moulton *et al.* [146] have proposed a Lagrangian approach that explicitly computes the intersection of the tag surfaces in two arbitrary frames. Tag surfaces are obtained by interpolating the tag curves that are stacked in different imaging planes. Surface intersections define a set of material lines for each time frame. These points were used to perform strain calculations employing a p-version of FE basis functions.

Radeva *et al.* [147] use two coupled volumetric models: a tissue deformation field and a model describing the LV geometry. The first model is represented by a cubic trivariate B-spline (coined *B-solid* by the authors); the second model is represented by two coupled surfaces (endocardium and epicardium) fitted to boundary points. It is assumed that the boundaries are either manually delineated or (semi)automatically detected from the tagged images. The B-solid is deformed under thin-plate internal constraints, and under two external forces. The first corresponds to tagging information: the iso-parametric curves of the model are deformed to align with the tag strips. Simultaneously, the B-solid is attracted toward the LV boundaries by integrating a distance function to edge points on the epicardial and endocardial surfaces. Therefore, in this method, boundary and tag information are incorporated in a unified approach. Since this method has been applied in combination with short-axis tagged images only, it yields in-plane 2-D displacements. In a recent paper, Huang *et al.* [149] have extended the method to analyze true 3-D deformations using a spatio-temporal model. The method differs from the one of Radeva *et al.*in that no boundary information is now incorporated. On the other hand, a spatio-temporal B-solid is constructed through a 4-D tensor product spline (3-D + t). The fitting process to SPAMM data is governed by a *normal constraint* which enforces the attraction produced by each tag plane to be in its normal direction. Since multiple, orthogonal tag planes are available, this allows a full 3-D reconstruction of the deformation field.

Kerwin and Prince [74] have developed an alternating projection technique to accurately estimate the 3-D location of the intersection points of the tag grid. The deformation field between two frames is recovered using thin-plate-spline interpo-

lation. Myocardial points are distinguished from those in static tissues by checking whether they pass across the imaging plane over time. In points that do not fulfill the previous criterion, a test is performed to check their inclusion within the outlined myocardial borders prior to rejection from the analysis. Such a rejection scheme is important for proper visualization and analysis of myocardial motion.

Recently, Young [148] has introduced the concept of *model tags* that represent the material surfaces within the heart tissue which are tagged with magnetic saturation. Model tags are "attached" to the heart and deform with it. They are embedded within a 3-D FE model describing the geometry of the LV; this model is linear in the transmural direction and employs bicubic Hermite interpolation in the circumferential and longitudinal directions. Instead of finding the 3-D location of the tag plane intersections, this approach finds the intersections of the model tags with the imaging planes (MTIs). The FE model is subsequently deformed so that the MTI match the tag stripes in each image plane. Matching is carried out by a local search algorithm guided by an orientation filter. Additionally mechanisms are incorporated to allow efficient user interaction and to correct for erroneous MTI matches.

b) Discrete models: Moore *et al.* [69] use MR tagging to reconstruct the location of material points through the cardiac cycle by interpolating the positions of the tags from short- and long-axis image planes using an iterative point-tracking algorithm. Discrete tag locations are arranged in cuboid volume elements which are identified in the deformed and reference frames. For each element, a 3-D strain tensor is calculated using the generalized inverse method [189]. Since the SA is performed on a coarse discrete grid, only average strains can be retrieved. The tag tracking procedure of this method compensates for through plane motion. An important conclusion from this work is that SA can be largely influenced by through plane motion if this is not corrected for.

Denney and Prince [73] employ a multidimensional stochastic approach to obtain a dense discrete model of the displacement field from a sparse set of noisy measurements (tag displacements). The displacement field is constrained to be smooth and incompressible (isochoric deformation). This formulation leads to a partial stochastic model of the deformation field that can be solved using Fisher's estimation framework [190].

V. Discussion

Comparison of the performance of different techniques is a difficult task due to the diversity of approaches, the different or complementary information obtained from them, the different imaging modalities and image acquisition protocols, and, last but not least, the lack of a standard way of reporting on performance. In order to draw some comparative conclusions, we have classified the existing methodologies according to the degree of their validation (Section V-A). At the same time, we introduce a number of performance criteria (Section V-B). In this comparison we have focussed on techniques leading to traditional cardiac indexes, *viz* global (Section III-A) and motion parameters (Section III-B). Table II summarizes this discussion.

A. Validation

Three main groups of papers can be distinguished: 1) with no evaluation or only qualitative illustrations, 2) with quantitative evaluation on nonhuman datasets, and 3) with quantitative evaluation on human datasets. This classification has been used in constructing Table II.

Although there are always exceptions confirming the rule, Table II indicates several trends. Most papers in the first category correspond to articles presenting technical or methodological aspects of advanced modeling techniques. The result sections in these papers are restricted to either technical aspects or proof-of-concept illustration on realistic images hypothesizing the potential of the technique. Only a few of them have seen follow-up articles confirming those hypotheses in large studies. Further evaluation of these techniques is required in order to determine their usefulness in clinical tasks.

Approaches in the second category are numerous. Methodologies in this category have been evaluated on simulated images or in phantom experiments. These have the advantage of providing ground truth to assess the accuracy and reproducibility of the techniques. Owing to the use of idealized geometries and measurement conditions, extrapolation of the results to *in vivo* human studies remains to be demonstrated. Some papers in this second category have evaluated their techniques on *ex vivo* or *in vivo* animal models. Several researchers have reported experiments with dogs [90], [101], [106], [108], [111]–[113], [124], [127], [129], [136], [139], swines [101], [108], [112], [146] or calfs [104], [192], [193].[10] Only a few studies have compared measurements, obtained from *ex vivo* [192], [193] or *in vivo* [101], [129], [150] animal studies, against other standard-of-reference techniques.

MR tagging techniques for reconstruction of myocardial motion or tissue deformation deserve separate attention. Most *in vivo* animal and human studies have reported on Monte Carlo analysis of sensitivity to errors in tag localization and tracking, and on the ability to recover the location of tags in different frames [69], [74], [145], [146], [191].[11] Several models have been used in the literature to benchmark the accuracy of motion and deformation recovery. These evaluations were based, for instance, on spherical and cylindrical models of cardiac motion [60], [69], [73], [145], FE solutions with realistic geometries [146], artificially generated motion trajectories [113] or synthetic images using the cardiac motion simulator [74], [149], [197] developed by Waks *et al.* [187] that builds upon the kinematic model of Arts *et al.* [198]. Recently, a study was carried out by Declerck *et al.* [199] that thoroughly compared four techniques [73], [145], [200], [201] for motion tracking from tagged MR. This paper provides results on normal and pathological subjects. Although the general trends of motion were captured correctly by all methods, this study shows that there

[10]Remarkably, a large amount of evaluations involving canine models have been acquired with the DSR. However, the reduced clinical availability of this technique and its specific image properties makes it difficult to extrapolate the results of the evaluation to other clinical imaging techniques.

[11]Validation MR tagging itself for describing tissue deformation has been addressed by Young [196] using a silicone gel phantom. Strains derived from MR tagging were compared to the analytic equilibrium strains under a Mooney–Rivlin material law.

are notable differences in the displacement and strain computations provided by each technique.

Finally, the third category includes studies that reported application on human volunteers and patients, including quantitative results in terms of cardiac functional parameters. The size of the populations in most of these studies was small. With only three exceptions, all studies were conducted on less than a dozen of subjects.

B. Performance Criteria

In the following subsections we elaborate on the criteria that we have used to compare the different methods.

1) Model Complexity or Flexibility: The complexity or flexibility of a technique has been categorized in four groups according to the number of DOFs[12] or parameters involved. 1) *Compact* models with only a few parameters (on the order of a dozen). Prototypical examples are superquadrics. 2) Flexible models with large number of DOFs and parameterized with *global*-support basis functions. Representative examples are harmonic parameterizations of several types. 3) Flexible models with large number of DOFs and parameterized with *local*-support basis functions. Members of this family are B-spline and polyhedral models. 4) Flexible *hierarchical* models encompassing a reduced set of DOFs coarsely describing shape, plus an extended set of DOFs giving extra flexibility to the model. Representative of this family are superquadrics with FFDs. Complexity is, to some extent, related to the computational demand of an algorithm. Highly flexible algorithms are usually related to higher computation time for deforming them to a given image dataset.[13] On the other hand, it is also a measure of the ability of a modeling technique to accommodate for fine shape details.

Although idealized models of ventricular geometry (mainly ellipsoids or ellipsoidal shells) are appealing for their parsimony and for historical reasons, Table II shows that no study has quantitatively demonstrated their accuracy in computing simple measurements as LVV and EF. Compact models have developed in two different directions. On one hand, in particular for the RV, some researchers have evaluated combinations of simple models that roughly derive RVV from a small number of linear measurements [104], [108]. The models, however, remain highly constrained and have been tested on *ex vivo* casts experiments only. A second direction has been to trade off the compactness of the superquadric models and their flexibility without the need of hierarchical decompositions [5], [6]. In this manner, flexibility is added in an elegant way by which each parameter function has an interpretation in terms of local and global shape changes.

Most approaches that reached the stage of quantitative evaluation are based on flexible or hierarchical representations. Both present challenges and advantages. Flexible representations (e.g., polyhedral meshes or harmonic decompositions) are highly versatile and can accommodate detailed shape variations. Most of the quantitative evaluation studies have been reported on local flexible models, most of which are able to cope even with complex topologies. On the other hand, restricting the space of possible shapes is usually difficult or requires substantial manual intervention or guidance [98], [99], [101], [143]. Hierarchical or top-down approaches aim at a reduction in computational time and at improving robustness by incrementally unconstraining the space of allowed shape variation [7]–[9], [33], [105], [107]. One weak point in hierarchical approaches is the need for *ad hoc* scheduling mechanisms to determine when one level in the representation hierarchy should be fixed and a new level added, and up to which level the model should be refined. Furthermore, optimization procedures involved in the recovery of hierarchical models have to be designed with particular care. It is unclear how it can be ensured that a succession of optimizations at different modeling levels actually leads to the optimum global deformation. Also, the question arises how to link different levels of model detail with the resolution of the underlying image data, and how to interact with the models if, after all, manual editing is required. Still, hierarchical model representations are an active and challenging field in 3-D medical image segmentation research where several investigators have presented encouraging results in cardiac [7]–[9], [107], [113], [122], [123] and thorax modeling [137], [202].

2) Robustness and Effective Automation: Processing prior to model recovery, automation of the recovery algorithm itself, and the presence of *ad hoc* parameters are factors that determine the *robustness* of a technique and its *effective automation*. By effective automation we refer to the automation of the overall approach, from raw images until the presentation of the functional parameters.

Before a given model can be fitted or deformed to a dataset, almost every technique requires some type of *preprocessing* to convert the raw grey-level images into a representation suitable for shape recovery. Section IV has suggested a classification of types of input data. For the sake of simplicity, Table II only indicates the degree of manual involvement to obtain the corresponding input data. Four categories were considered: (N) no preprocessing required, (I) manual initialization of landmarks/models, (A) (semi) automated initialization of landmarks/models integrated into the technique, and (M) fully manual segmentation of landmarks/contours. Although variability inherent to the preprocessing can have a marked effect on the overall performance of a technique, this factor is usually disregarded in the evaluation of algorithms. A remarkable exception is the evaluation of MR tag tracking algorithms using Monte Carlo analysis to assess the influence of erroneous tag localization in the recovery of tissue deformation [69], [74], [145], [146], [191]. Model initialization is also related to the issue of preprocessing. Although a few techniques make explicit mention of the procedure required to initialize the model (cf., e.g., [5], [6], [72], [132], [136], and [137]), model initialization in a 3-D environment can be nontrivial or require expert guidance.

Another factor undermining robustness and reliability of a technique, is the presence of *ad hoc parameters* that have to

[12]Here, we disregard the obvious rigid transformation parameters to instantiate the model in world coordinates.

[13]Actually, it is the conjunction of model parameterization and the recovery strategy which determines the computational load of an approach. It would have been very interesting to report computation time with each technique. Unfortunately, variability in hardware architecture over time and techniques renders any quantitative comparison unrealistic.

be set by the user. This can be particularly problematic when such parameters are highly dependent on a given dataset. This is a known problem, for instance, of many physics-based deformable models for which several weights must be tuned to balance the smoothing constraints to the external energy terms. However, in the literature, analysis of sensitivity of the result to the weighting parameters is mostly missing. In Table II, we have classified the different techniques into two categories according to the presence of user-defined *ad hoc* parameters: $(-)$ no parameters or parameters with corresponding analysis of sensitivity, and $(+)$ parameters for which no sensitivity analysis was performed. The fact that several methods do not present *ad hoc* parameters $(-)$ does not have to be confounded with overall robustness. Even within the approaches with quantitative evaluation, many papers in the $(-)$ category either require substantial preprocessing [9], [25], [26], [68], [145], [146], [150], [151] or human guidance [98], [99], [104], [108], [116], [117], [179]. Both factors influence the robustness and reproducibility of the derived functional information.

Finally, Table II also indicates the degree of user guidance (*automation*) of the fitting procedures for given input data (preprocessing) and set of *ad hoc* parameters. Three degrees of automation were used to classify the approaches: $(=)$ relying on substantial human guidance, $(-)$ manual interaction can be necessary for guiding/correcting the deformation, and $(+)$ fully automated. In general terms, the larger the need for human intervention during the fitting procedure, the less robust a technique will become, and the more prone it will be to interobserver/intraobserver variability of the final results.

VI. Conclusions and Suggestions for Future Research

In this paper, we have reviewed techniques for 3-D geometric modeling and analysis of cardiac images. In particular, we have focussed on those techniques leading to traditional indexes of cardiac function. We have proposed a systematic classification of the approaches based on the type of representation of the geometric model, and the type of input data required for model recovery (Table I). Furthermore, we have given a critical assessment of these approaches according to the type of functional parameters that they provide, their degree of evaluation, and the performance achieved in terms of modeling flexibility, complexity, and effective automation (Table II).

From the surveyed literature, four main lines of future efforts can be distinguished.

1) Research on Modeling and Model deformation Techniques: The last two decades have witnessed an enormous amount of efforts in 3-D models of LV and RV. This holds true for all imaging modalities (cf. Table I). In spite of the large number of attempts, no approach has simultaneously achieved robustness, automation, model flexibility and computational speed. Manual outlining and analysis of cardiac images is still the most popular technique in clinical environments.

Several issues will require more attention in order to integrate the advances of modeling techniques into clinical practice. Accurate 3-D modeling techniques are, in general, computationally intensive. Exploration of flexible modeling techniques that make an efficient use of their DOFs will be worthy of further research. So far the main flow of efforts has been focussed on adopting generic geometrical representations to build cardiac shape models (e.g., superquadrics, B-splines, polyhedral meshes, Fourier descriptors, etc.). As a consequence, in generating a realistic LV shape, the representations are either too restrictive or require a considerable amount of parameters. The question arises of how to infer a compact representation giving rise to realistic shapes, possibly learned from examples.[14] Modeling approaches that go from shape examples to a specific shape representation can reduce computational demands and improve their robustness. A small number of efficiently selected model parameters reduces the dimensionality of the model recovery problem, and naturally constrains its results owing to model specificity.

Further investigation of suitable image features will be needed to improve shape recovery. In particular, incorporation of domain knowledge about the type of image modality (and acquisition protocols) can play an important role in increasing the accuracy of shape recovery techniques.

Most of the modeling techniques presented in this review were either purely geometric or inspired in a *virtual* physical analog (physics-based approaches). Recently, a few papers have introduced known biomechanical properties of the heart in the formulation of models that analyze cardiac images [142], [150]–[152]. Further development of such approaches, and their application to segmentation tasks, can be a natural way of extending the ideas of physics-based methods and of relating some of the *ad hoc* parameters with experimental evidence provided by biomechanics.

2) Research on Interactive Model-Based Segmentation: Table II supports the idea that model-based cardiac segmentation has not reached the status of being effectively automated since current techniques either require substantial expert guidance, *ad hoc* parameter fine-tuning or nontrivial preprocessing. Although full automation is a desirable end goal, its difficulty has been acknowledged many times in the literature. There is a growing consensus that user interaction is, to some extent, unavoidable, and that it has to be considered as an integrated part of the segmentation procedure. Therefore, development of efficient tools for 3-D interaction will play an important role in the near future. "Efficient" entails that with minimal and intuitive user interaction the operator keeps control over the segmentation process to correct or overrule its results where it has failed, and to guide the algorithm in abnormal situations (e.g., in front of a pathological case). Of course, the issue of reproducibility in case of human intervention needs attention. Where well-defined repetitive tasks are recognized, or where a local user interaction can be extrapolated to a broader area, the process should be automated, thus improving segmentation throughput and repeatability. How to devise such efficient and intuitive mechanisms for 3-D manipulation of models and volumetric data, and how to integrate them into the deformation of the models remain topics of future research.

[14]An interesting approach is to extract statistical models from sample shapes [203] and to capture the most representative DOFs via principal component analysis. Although interesting results have been obtained in 2-D applications, more research is needed to solve practical problems in their 3-D extensions.

3) Research on Functional Cardiac Descriptors: There are many shape and motion parameters other than traditional indexes (cf. Appendix A). Unfortunately, although these new indexes seem to provide richer information and/or a more detailed analysis of cardiac function, their clinical evaluation has been very limited. As a consequence, it is difficult to determine their clinical relevance and the extra information provided with respect to traditional indexes like LVV, EF, etc. The lack of clinical evaluations may be related to the fact that advanced 3-D modeling techniques, from which these parameters can be derived, are computationally expensive and require considerable user intervention. The need of considerable preprocessing and postprocessing procedures, *ad hoc* parameter settings and technical understanding of the modeling technique itself may explain why most of the described approaches are not available as stand-alone prototypes on which clinical studies can be carried out routinely.

There is certainly place for development of novel shape and motion descriptors. However, there is even a larger need for evaluation of already existing indexes on reference data sets and/or large scale clinical studies. It is remarkable that this lack of large evaluation studies is present even in many techniques aiming at the extraction of traditional functional parameters (Table II).

It is unrealistic to expect that every new technique proposed in the future will go through the process of a thorough clinical evaluation study. Unfortunately, many research institutes working on geometric modeling and shape analysis are not located in a clinical environment. Access to state-of-the-art image material and derived parameters for testing and benchmarking purposes is, therefore, difficult. In this respect, a public, common database of a representative set of images from different modalities would be highly beneficial. This database should establish a few standard data sets (both synthetic and clinical study cases) with as much independent measurements as possible of mass, SV, etc. With the current speed of development in the imaging modalities, such a database should be updated regularly to be representative of the state-of-the-art imaging technology.

4) Multidisciplinary Approaches: When imaging and modeling techniques get more complex, the interplay of clinicians, medical physicists, and technologists in a common environment becomes increasingly important. Several issues have to be addressed in a cooperative fashion: the interrelationship between image acquisition and cardiac modeling, the development of effective visualization techniques of 4-D datasets, realization of intuitive interfaces to interact with geometric models at the various stages of initialization, deformation and eventual correction of results, and concise transferal of clinical information from images/models to the cardiologists.

It is to be expected that approval by clinicians of a model-based technique that provides functional parameters will depend on close collaboration between technicians involved in image acquisition, computer scientists devoted to the development of efficient modeling and model recovery techniques, and cardiologists providing feedback about the desired information and display methods, the validity of the assumptions and the design of evaluation studies.

APPENDIX A
NONTRADITIONAL SHAPE AND MOTION DESCRIPTORS

Three-dimensional model-based analysis of LV shape and motion has the potential of providing rich morphological and functional information. Current clinical assessment of cardiac function is based mainly on global parameters as LVV and EF. However, several researchers have demonstrated in the past the importance of local functional indexes as WT and segmental motion analysis [93], [204]–[206], and local curvature and shape [50]–[53] as potential CIs. Unfortunately, most of these studies were based on 2-D imaging techniques. Although they can indicate major trends about cardiac shape, a 3-D analysis would be beneficial to better account for the true cardiac geometry. In this section, we briefly summarize several new indexes proposed in the literature to describe shape and/or motion. Some of these indexes have been presented as a by-product of a specific modeling technique while others are easily computable from any model representation. Therefore, this distinction seems a natural classification.

A. Generic Descriptors

Mean and Gaussian Curvature: The principal curvatures (k_1 and k_2, respectively) measure the maximum and minimum bending of a regular surface. Rather than using principal curvatures, it is more common to use two derived quantities known as Gaussian ($K = k_1 k_2$) and mean ($H = (k_1 + k_2)/2$) curvatures. By analyzing the signs of the pair (K, H) it is possible to locally distinguish between eight surface types [207].

Friboulet *et al.* [88] have studied the distribution of the Gaussian curvature in the LV at different phases of the cardiac cycle. From this study it was concluded that this distribution remains structurally stable over time. Whereas the LV free wall provides rich and dense curvature information, the curvature at the septal wall is less suitable to establish point correspondences. Similar findings were made by Sacks *et al.* [106] with respect to the RV free wall: the RV free wall has relatively uniform distribution of principal curvatures, and the surface geometry of the RV free wall does not change significantly from end diastole to end systole.

Shape Index and Shape Spectrum: Although mean and Gaussian curvatures are related to the concept of curvedness, there still remains scale information in these shape descriptors. To overcome this problem, Clarysse *et al.* [208] have used the *shape index* (s) and the *curvedness* (c), two parameters that were introduced by Koenderink and van Doorn [209] and are defined as follows:

$$s = \frac{2}{\pi} \tan^{-1} \frac{k_2 + k_1}{k_2 - k_1} \tag{11}$$

$$c = \left(\frac{k_1^2 + k_2^2}{2} \right)^{\frac{1}{2}}. \tag{12}$$

While c is inversely proportional to the object size, s defines a continuous distribution of surface types ranging from cup-like umbilic $(s = -1)$ to peak-like umbilic $(s = 1)$ points. It can be shown that while the shape index is invariant by homothecy, the

curvedness is not. In this way, shape information and size can be easily decoupled.

The *shape spectrum* [210], $\gamma(h,t)$, is a global shape index defined as the fractional area of the LV with shape index value h, at time t

$$\gamma(h,t) = \frac{1}{A}\iint_S \delta(s(\mathbf{x}) - h)\, dS \tag{13}$$

where

$A = \iint_S dS$	total area of the surface S;
dS	small region around the point $\mathbf{x}$;
$\delta(\cdot)$	1-D Dirac delta function.

Cardiac deformation can be analyzed by tracking the shape index and curvedness of *SSPs* over time. SSPs are connected surface patches whose points have similar shape indexes, i.e., the shape index falls within a given range $s \pm \Delta s$. Clarysse *et al.*have shown the potential applicability of these indexes by analyzing phantoms of normal and diseased LVs. A LV model of dilated cardiomyopathy, and a model of an ischemic LV (both akinetic and hypokinetic in the left anterior coronary territory) were generated using 4-D spherical harmonics. The curvedness spectrum was significantly altered by both pathologies, even when they were localized (ischemic models). Reduction of the global function in the dilated myocardium had no significant repercussion on the shape index spectra. This could be an indicator that this pathology mostly affects the magnitude of motion only. An alternative to global analysis is to track the curvature parameters in predetermined regions. Clarysse *et al.* have tracked three reference points over time: the apex, a point in the anterior wall, and a point in the cup of the pillar anchor. Using the local temporal variation of the curvedness and shape index, it was possible to distinguish between the normal and diseased model. A potential problem of this techniques is the reliable tracking of SSPs. If local deformations are too large the trace of points might be lost.

Local stretching: Mishra *et al.* [87] have presented a computational scheme to derive local epicardial stretching under conformal motion. In conformal motion, it is assumed that motion can be described by a spatially-variant but locally isotropic stretching factor. In particular, for any two corresponding patches before and after motion, P and $\bar{P}$, the *local stretching factor*, τ, can be computed from the change in Gaussian curvature and a polynomial stretching model by means of the relationship

$$\bar{K} = \frac{K}{\tau^2} + \frac{f(E,F,G,\tau,\tau_u,\tau_v,\tau_{uu},\tau_{vv})}{\tau^2} \tag{14}$$

where

$f(\cdot)$	polynomial stretching model (linear or quadratic in [87]);
E, F, and G	coefficients of the first fundamental form [211];
(u,v)	coordinates of a local parameterization of the surface patch.

Mishra *et al.* [87] present a method to solve for τ in (14) and show that the local epicardial stretching factors computed over the cardiac cycle follow a similar evolution to the temporal variation of the principal strains obtained by Young *et al.* [100] using SA techniques.

B. Model-Specific Shape Descriptors

Geometric Cardiogram (GCG): Azhari *et al.* [212] describe a method for classification of normal and abnormal LV geometries by defining a "geometrical cardiogram" (GCG), a helical sampling of the LV geometry from apex to base [213]. The GCG at end systole and at end diastole are subsequently analyzed via a KLT to compress their information. A truncated set of the KLT basis vectors is used to project the GCG of individual patients into a lower dimensional space, and the mean square error between the projected and original GCG is used to discriminate between normal and abnormal LV [214]. From this vectorial representation LVV and EF [213], and WT [91] can also be computed.

Deformable Superquadric and Related Models: One of the first 3-D primitives used to model the LV was the superquadric. It is a natural extension of the simplified geometric models originally used in 2DE [14] and angiocardiography [10]–[13]. Along with three main axes indicating principal dimensions, the superquadric models can be endowed with additional parametric deformations as linear tapering and bending [9], [109], FFDs [113], displacement fields [7], [8] or parametric functions providing information about radial and longitudinal contraction, twisting motion, and deformation of the LV long-axis [5], [6] and wall thickness [6]. In particular, Park *et al.* [5], [6] suggest to decompose deformation and motion into a few parametric functions that can be presented to the clinician in the form of simple plots. All these functions are either independent of the total LV volume (e.g., twisting) or can be normalized with respect to the dimensions of the LV (e.g., radial and longitudinal contraction). This allows interpatient comparisons of contraction and shape change.

Global motion analysis based on departure from an affine model: Friboulet *et al.* [119] modeled the LV using a polyhedral mesh at each frame of the cardiac cycle. The state of the LV was characterized by the center of gravity and the moments of inertia of the polyhedral mesh. The deformation between two frames was hypothesized to follow an affine model. By defining a metric to compare two different polyhedral representations, the authors were able to quantify the difference between the actual interframe deformation and the corresponding deformation derived from an affine motion model. Several parameters of global motion are then derived: the temporal variation of the longitudinal and transversal moments of inertia, and the proportion of total motion explained by the affine model. By means of case studies it was demonstrated that these global indexes are able to discriminate between normal $(\mathrm{EF} = 0.71)$ and highly diseased $(\mathrm{EF} = 0.1)$ LVs. On the other hand, the global nature of these indexes precludes the quantification of localized, inhomogeneous dysfunction of the LV.

Motion decomposition through planispheric transformation: Declerck *et al.* [114] have proposed a canonical decomposition of cardiac motion into three components: radial motion, twisting motion around the apico-basal axis, and long-axis shortening. This decomposition is achieved through

a transformation of the Cartesian coordinates of the LV wall to a planispheric space. In this space, a 4-D transformation is defined that regularly and smoothly parameterizes the spatio-temporal variation of the LV wall. Since the canonical decomposition of motion can be directly obtained in the planispheric space, these descriptors also vary smoothly along the cardiac cycle. Finally, by tracking the position of material points over time in the planispheric space and subsequent mapping to Cartesian coordinates, it is possible to reconstruct their 3-D trajectories.

Modal analysis—deformation spectrum: Nastar and Ayache have introduced the concept of *deformation spectrum* [127] which can be applied within the framework of modal analysis [153]. The deformation spectrum is the graph representing the value of the modal amplitudes as a function of mode index. The deformation spectrum corresponding to the deformation between two image frames describes which modes are excited in order to deform one object into another. It also gives an indication of the strain energy [127] of the deformation. As a consequence, a pure rigid deformation has zero strain energy. Two deformations are said to be *similar* when the corresponding deformation fields are equivalent up to a rigid transformation. In order measure the dissimilarity of two deformation fields, the lower-order modes related to rigid transformation are discarded. The difference of the deformation spectra so computed, can be used to define a metric between shapes (e.g., the LV in two phases of the cardiac cycle) that can be applied to classify them into specific classes (e.g., normal/abnormal motion patterns). Finally, the amplitude of the different modes can be tracked over time. Using Fourier spectral analysis, Nastar and Ayache have shown that these modes concentrate in a few low-frequency coefficients.

APPENDIX B
MR TAG LOCALIZATION TECHNIQUES

Early attempts to model myocardial tissue deformation tracked tag grid intersections manually over time [68]. Other researchers [69], [73], [74], [141], [145], [191] have used semiautomatic tools [215]–[217], based on *snakes*, to locate and track tag intersections and to define myocardial contours. Although they still require user interaction, these tools can speed up the manual procedure while reducing interobserver variability [218].

Young *et al.* [72] propose an interactive scheme for tag tracking. The 2-D tag grid is modeled as a whole (*active carpet*). Separate manual segmentation of the LV boundaries is required to compute myocardial strains only. Tag tracking is performed using a modified *snake* [168] algorithm. Since tags show up in these images as dark lines (intensity valleys), the image intensity is used as external energy. Additionally interactive guidance is supported by introducing user-defined constrains. Only points in the myocardium mask are tracked in each frame while carpet points outside the myocardium (*inactive points*) provide a weak form of continuity. Kraitchman *et al.* [188] have introduced an interactive method for tracking tag intersections. The method shares some features of the *active carpet* model of Young *et al.* [72]. The carpet of tag intersections is modeled as a mass-spring mesh of triangles. Tag intersections are tracked by means of a correlation-based external energy and, eventually, adding interactive constraints. Finally, this technique allows to compute average strains on the triangular patches. Another method for automatic tracking of the SPAMM grid has been presented by Kumar and Goldgof [70]. In the first frame, template matching is applied to provide an initial position of the tag grid. In this frame, the tag grid has a high contrast and a regular arrangement. In the subsequent frames, each line of the tag grid is independently tracked using a discrete *thick snake* with a width of two pixels (the typical tag width). The product of the image intensity in the two pixels is used as external energy to attract the snakes to the tag lines. Although these methods for extracting tag intersections can be useful for 3-D deformation analysis, in the original formulations, the methods proposed in [72], [188], and [70] have all been applied to 2-D SA.

There exist other approaches not based on snakes. Zhang *et al.* [219] decouple horizontal and vertical tag tracking via Fourier decomposition and spectral masking. In order to compensate for spectral cross modulation from perpendicular lines, local histogram equalization is needed prior to spectral analysis. Detection of tag lines is simplified in the preprocessed images and a simple local search can then be used to track local intensity minima (tag lines) over time. Kerwin and Prince [197] have developed a method to simultaneously detect and track tag surfaces without the need for prior 2-D tag tracking. Tag surfaces are modeled using a *kriging update model* [220], [221]. This model parameterizes tag surfaces using a global quadratic surface plus a local stochastic displacement. A recursive spatio-temporal scheme is developed that updates the kriging model. Measurements to update the model are obtained through a local search for tag lines. In this search, a matched filter is employed modeling the intensity profile across a tag line. Recently, Osman *et al.* [222], [223] have introduced and evaluated a method for cardiac motion tracking based on the concept of HARP. The method uses isolated spectral peaks in the Fourier domain of MR tagged images as a cue for tag tracking. The inverse Fourier transform of a spectral peak is a complex image whose computed angle is called HARP image. In Osman *et al.* [222], [224] it is shown how this angle can be treated as a material property that can be related to myocardial strain. This technique has the advantage that is fast, fully automatic and provides dense material properties. So far the method has been applied to 2-D images and, thus, only provides information about "apparent motion." In Osman and Prince *et al.* [225], the authors present several visualization techniques that can be used to display the information provided by HARP images.

REFERENCES

[1] American Heart Association, 1999 Heart and Stroke Statistical Update (1998). [Online]. Available: http://www.americanheart.org
[2] M. L. Simoons, "The european heart survey: Inventory of the care of cardiovascular diseases," presented at the XXIst Eur. Soc. Cardiology Congress, Barcelona, Catalonia, 1999. Presentation of the ESC President Elect.
[3] T. McInerney and D. Terzopoulos, "Deformable models in medical image analysis: A survey," *Med. Image Anal.*, vol. 1, no. 2, pp. 91–108, June 1996.

[4] A. Singh, D. Goldgof, and D. Terzopoulos, Eds., *Deformable Models in Medical Image Analysis*. Los Alamitos, CA: IEEE Comput. Soc. Press, 1998.

[5] J. Park, D. N. Metaxas, and L. Axel, "Analysis of left ventricular wall motion based on volumetric deformable models and MRI-SPAMM," *Med. Image Anal.*, vol. 1, no. 1, pp. 53–72, Mar. 1996.

[6] J. Park, D. N. Metaxas, A. A. Young, and L. Axel, "Deformable models with parameter functions for cardiac motion analysis from tagged MRI data," *IEEE Trans. Med. Imag.*, vol. 15, pp. 278–289, June 1996.

[7] T. O'Donnell, A. Gupta, and T. Boult, "The hybrid volumetric ventriculoid: New model for MR-SPAMM 3-D analysis," in *IEEE Comput. in Cardiol.*. Vienna, Austria, Sept. 1995, pp. 5–8.

[8] T. O'Donnell, T. Boult, and A. Gupta, "Global models with parametric offsets as applied to cardiac motion recovery," in *Comput. Vis. Pattern Recogn.* San Francisco, CA, June 1996, pp. 293–299.

[9] E. Bardinet, L. D. Cohen, and N. Ayache, "A parametric deformable model to fit unstructured 3D data," *Comput. Vis. Image Underst.*, vol. 71, no. 1, pp. 39–54, July 1998.

[10] J. W. Kennedy, W. A. Baxley, M. M. Figley, H. T. Dodge, and J. R. Blackmon, "Quantitative angiocardiography: I. The normal left ventricle in man," *Circulation*, vol. 34, pp. 272–278, Aug. 1966.

[11] H. J. Hermann and S. H. Bartle, "Left ventricular volumes by angiocardiography: Comparison of methods and simplification of techniques," *Cardiovasc. Res.*, vol. 2, no. 4, pp. 404–414, Oct. 1968.

[12] J. C. Davila and M. E. Sanmarco, "An analysis of the fit of mathematical models applicable to the measurement of left ventricular volume," *Amer. J. Cardiol.*, vol. 18, pp. 31–42, July 1966.

[13] H. T. Dodge, H. Sandler, W. A. Baxley, and R. R. Hawley, "Usefulnes and limitations of radiographic methods for determining left ventricular volume," *Amer. J. Cardiol.*, vol. 18, pp. 10–24, July 1966.

[14] C. Vuille and A. E. Weyman, "Left ventricle I: General considerations, assessment of chamber size and function," in *Principles and Practice of Echocardiography*, 2nd ed, A. E. Weyman, Ed. Philadelphia, PA: Lea and Febiger, 1994.

[15] M. J. Raphael and R. M. Donaldson, "The normal heart: Methods of examination," in *Textbook of Radiology and Imaging*, 6th ed, D. Sutton, Ed. New York: Churchill Livingstone, 1998, pp. 541–565.

[16] H. A. McCann, J. C. Sharp, T. M. Kinter, C. N. McEwan, C. Barillot, and J. F. Greenleaf, "Multidimensional ultrasonic imaging for cardiology," *Proc. IEEE*, vol. 76, pp. 1063–1071, Sept. 1988.

[17] T. R. Nelson, D. B. Downey, D. H. Pretorius, and A. Fenster, *Three-Dimensional Ultrasound*. Philadelphia, PA: Lippincott Williams & Wilkins, 1999.

[18] R. A. Robb, E. A. Hoffman, L. J. Sinak, L. D. Harris, and E. L. Ritman, "High-speed three-dimensional X-ray computed tomography: The dynamic spatial reconstructor," *Proc. IEEE*, vol. 71, pp. 308–319, Mar. 1983.

[19] D. P. Boyd and M. J. Lipton, "Cardiac computed tomography," *Proc. IEEE*, vol. 71, pp. 298–307, Mar. 1983.

[20] C. B. Higgins, "Overview of MR of the heart—1986," *Amer. J. Roentgenol.*, vol. 146, no. 5, pp. 907–918, May 1986.

[21] G. A. Wright, "Magnetic resonance imaging," *IEEE Signal Processing Mag.*, pp. 56–66, Jan. 1997.

[22] J. U. Quistgaard, "Signal acquisition and processing in medical diagnostic ultrasound," *IEEE Signal Processing Mag.*, pp. 67–74, Jan. 1997.

[23] M. Ariet, E. A. Geiser, S. M. Lupkiewicz, D. A. Conetta, and C. R. Conti, "Evaluation of a three-dimensional reconstruction to compute left ventricular volume and mass," *Amer. J. Cardiol.*, vol. 54, no. 3, pp. 415–420, Aug. 1984.

[24] G. Treece, R. Prager, A. Gee, and L. Berman, "Volume measurements in sequential freehand 3-D ultrasound," in *Lecture Notes in Computer Science*, A. Kuba, M. Sámal, and A. Todd-Pokropek, Eds. Berlin, Germany: Springer-Verlag, 1999, vol. 1613, Inform. Processing Med. Imag., pp. 70–83.

[25] A. S. Gopal, D. L. King, J. Katz, L. M. Boxt, D. L. King Jr., and M. Y. Shao, "Three-dimensional echocardiographic volume computation by polyhedral surface reconstruction: *In vitro* validation and comparison to magnetic resonance imaging," *J. Amer. Soc. Echocardiogr.*, vol. 5, no. 2, pp. 115–124, Mar. 1992.

[26] M. E. Legget, D. F. Leotta, E. L. Bolson, J. A. McDonald, R. W. Martin, X. N. Li, C. M. Otto, and F. H. Sheehan, "System for quantitative three dimensional echocardiography of the left ventricle based on magnetic field position and orientation sensing system," *IEEE Trans. Biomed. Eng.*, vol. 45, pp. 494–504, Apr. 1998.

[27] G. Coppini, R. Poli, and G. Valli, "Recovery of the 3-D shape of the left ventricle from echocardiographic images," *IEEE Trans. Med. Imag.*, vol. 14, pp. 301–317, June 1995.

[28] G. D. Stetten and S. M. Pizer, "Medial-node models to identify and measure objects in real-time 3-D echocardiography," *IEEE Trans. Med. Imag.*, vol. 18, pp. 1025–1034, Oct. 1999.

[29] J. Maehle, K. Bjoernstad, S. Aakhus, H. G. Torp, and B. A. Angelsen, "Three-dimensional echocardiography for quantitative left ventricular wall motion analysis: A method for reconstruction of endocardial surface and evaluation of regional dysfunction," *Echocardiography*, vol. 11, no. 4, pp. 397–408, 1994.

[30] G. Germano, J. Erel, H. Kiat, P. B. Kavanagh, and D. S. Berman, "Quantitative LVEF and qualitative regional function from gated 201-T1 perfusion SPECT," *J. Nucl. Med.*, vol. 38, no. 5, pp. 749–754, May 1997.

[31] T. L. Faber, E. M. Stokely, G. H. Templeton, M. S. Akers, R. W. Parkey, and J. R. Corbett, "Quantification of three-dimensional left ventricular segmental wall motion and volumes from gated tomographic radionuclide ventriculograms," *J. Nucl. Med.*, vol. 30, no. 5, pp. 638–649, May 1989.

[32] T. L. Faber, M. S. Akers, R. M. Peshock, and J. R. Corbett, "Three-dimensional motion and perfusion quantification in gated single-photon emission computed tomograms," *J. Nucl. Med.*, vol. 32, no. 12, pp. 2311–2317, Dec. 1991.

[33] G. Germano, P. B. Kavanagh, and D. S. Berman, "An automatic approach to the analysis, quantitation and review of perfusion and function from myocardial perfusion SPECT images," *Int. J. Card. Imag.*, vol. 13, no. 4, pp. 337–346, Aug. 1997.

[34] B. Ohnesorge, T. Flohr, C. Becker, A. Knez, A. F. Kopp, K. Fukuda, and M. F. Reiser, "Cardiac imaging with rapid, retrospective ECG synchronized multilevel spiral CT" (in German), *Der Radiologe*, vol. 40, no. 2, pp. 111–117, Feb. 2000.

[35] K. Klingenbeck-Regn, S. Schaller, T. Flohr, B. Ohnesorge, A. F. Kopp, and U. Baum, "Subsecond multislice computed tomography: Basics and applications," *Eur. J. Radiol.*, vol. 31, no. 2, pp. 110–124, Aug. 1999.

[36] D. P. Boyd and C. Haugland, "Recent progress in electron beam tomography," *Med. Imag. Tech.*, vol. 11, pp. 578–585, 1993.

[37] *J. Magn. Reson. Imag. (Special Issue: Cardiovascular MRI)*, vol. 10, no. 5, Nov. 1999.

[38] A. M. Keller, R. M. Peshock, C. R. Malloy, L. M. Buja, R. Nunnally, R. W. Parkey, and J. T. Willerson, "In vivo measurement of myocardial mass using nuclear magnetic resonance imaging," *J. Amer. Coll. Cardiol.*, vol. 8, no. 1, pp. 113–137, July 1986.

[39] G. B. Cranney, C. S. Lotan, L. Dean, W. Baxley, A. Bouchard, and G. M. Pohost, "Left ventricular volume measurement using cardiac axis nuclear magnetic resonance imaging," *Circulation*, vol. 82, no. 1, pp. 154–163, July 1990.

[40] M. C. Dulce, G. H. Mostbeck, K. K. Friese, G. R. Caputo, and C. B. Higgings, "Quantification of the left ventricular volumes and function with cine MR imaging: Comparison of geometric models with three-dimensional data," *Radiology*, vol. 188, no. 2, pp. 371–376, Aug. 1993.

[41] R. J. van der Geest, A. de Roos, E. E. van der Wall, and J. H. C. Reiber, "Quantitative analysis of cardiovascular MR images," *Int. J. Card. Imag.*, vol. 13, no. 3, pp. 247–258, June 1997.

[42] C. H. Lorenz, E. S. Walker, V. L. Morgan, S. S. Klein, and T. P. Graham Jr., "Normal human right and left ventricular mass, systolic function, and gender differences by cine magnetic resonance imaging," *J. Cardiovasc. Magn. Res.*, vol. 1, no. 1, pp. 7–21, 1999.

[43] J. T. Marcus, M. J. W. Götte, L. K. de Waal, M. R. Stam, R. J. van der Geest, R. M. Heethaar, and A. C. van Rossum, "The influence of through-plane motion on left ventricular volumes measured by magnetic resonance imaging: Implications for image acquisition and analysis," *J. Cardiovasc. Magn. Res.*, vol. 1, no. 1, pp. 1–6, 1999.

[44] R. Beyar, E. P. Shapiro, W. L. Graves, W. J. Rogers, W. H. Guier, G. A. Carey, R. L. Soulen, E. A. Zerhouni, M. L. Weisfeldt, and J. L. Weiss, "Quantification and validation of left ventricular wall thickening by a three-dimensional volume element magnetic resonance imaging approach," *Circulation*, vol. 81, no. 1, pp. 297–307, Jan. 1990.

[45] E. R. McVeigh, "MRI of myocardial function: Motion tracking techniques," *Magn. Reson. Imag.*, vol. 14, no. 2, pp. 137–150, 1996.

[46] N. R. Clark, N. Reichek, P. Bergey, E. A. Hoffman, D. Brownson, L. Palmon, and L. Axel, "Circumferential myocardial shortening in the normal human left ventricle. Assessment by magnetic resonance imaging using spatial modulation of magnetization," *Circulation*, vol. 84, no. 1, pp. 67–74, July 1991.

[47] E. A. Zerhouni, D. M. Parish, W. J. Rogers, A. Yang, and E. P. Shapiro, "Human heart: Tagging with MR imaging—A method for noninvasive assessment of myocardial motion," *Radiology*, vol. 169, no. 1, pp. 59–63, Oct. 1988.

[48] L. Axel and L. Dougherty, "Heartwall motion: Improved method of spatial modulation of magnetization for MR imaging," *Radiology*, vol. 172, no. 2, pp. 349–350, Aug. 1989.

[49] K. T. Weber and E. W. Hawthorne, "Descriptors and determinants of cardiac shape: An overview," *Fed. Proc.*, vol. 40, no. 7, pp. 2005–2010, May 1981.

[50] G. B. Mancini, S. F. De Boe, E. Anselmo, S. B. Simon, M. T. Le Free, and R. A. Vogel, "Quantitative regional curvature analysis: An application of shape determination for the assessment of segmental left ventricular function in man," *Amer. Heart J.*, pt. 1, vol. 113, no. 2, pp. 326–334, Feb. 1987.

[51] G. B. J. Mancini, S. F. DeBoe, M. J. McGillem, and E. R. Bates, "Quantitative regional curvature analysis: A prospective evaluation of ventricular shape and wall motion measurements," *Amer. Heart J.*, pt. 1, vol. 116, no. 6, pp. 1611–1621, Dec. 1988.

[52] D. A. Kass, T. A. Traill, M. Keating, P. I. Altieri, and W. L. Maughan, "Abnormalities of dynamic ventricular shape change in patients with aortic and mitral valvular regurgitation: Assessment by Fourier shape analysis and global geometric indexes," *Circ. Res.*, vol. 62, no. 1, pp. 127–138, Jan. 1988.

[53] G. Barletta, M. Baroni, R. del Bene, A. Toso, and F. Fantini, "Regional and temporal nonuniformity of shape and wall movement in the normal left ventricle," *Cardiology*, vol. 90, no. 3, pp. 195–201, Dec. 1998.

[54] C. Kondo, G. R. Caputo, R. Smelka, E. Foster, A. Shimakawa, and C. B. Higgins, "Right and left ventricular stroke volume measurements with velocity-encoded cine MR imaging: *In vitro* and *in vivo* validation," *Amer. J. Roentgenol.*, vol. 157, no. 1, pp. 9–16, July 1991.

[55] L. D. Hillis, B. G. Firth, and M. D. Winniford, "Analysis of factors affecting the variability of Fick versus indicator dilution measurements of cardiac output," *Amer. J. Cardiol.*, vol. 56, no. 12, pp. 764–768, Nov. 1986.

[56] J. C. McEachen, A. Neohorai, and J. S. Duncan, "A recursive filter for temporal analysis of cardiac motion," in *Proc. Math. Meth. Biomed. Imag. Anal.*, Seattle, WA, 1994, pp. 124–133.

[57] M. J. Potel, J. M. Rubin, S. A. MacKay, A. M. Aisen, J. Al-Sadir, and R. E. Sayre, "Methods for evaluating cardiac wall motion in three dimensions using bifurcation points of the coronary arterial tree," *Inv. Rad.*, vol. 18, no. 1, pp. 47–57, Jan. 1983.

[58] H. C. Kim, B. G. Min, M. M. Lee, J. D. Seo, Y. W. Lee, and M. C. Han, "Estimation of local cardiac wall deformation and regional wall stress from biplane coronary cineangiograms," *IEEE Trans. Biomed. Eng.*, vol. 32, pp. 503–512, July 1985.

[59] C. W. Chen and T. S. Huang, "Epicardial motion and deformation estimation from coronary artery bifurcation points," in *Proc. Int. Conf. Comput. Vis.*, Osaka, Japan, Dec. 1990.

[60] A. A. Young, P. J. Hunter, and B. H. Smaill, "Estimation of epicardial strain using the motions of coronary bifurcations in biplane cineangiography," *IEEE Trans. Biomed. Eng.*, vol. 39, pp. 526–531, May 1992.

[61] D. C. Harrison, A. Goldblatt, E. Braunwald, G. Glick, and D. T. Mason, "Studies on cardiac dimensions in intact unanesthetized man. I. Description of techniques and their validation," *Circ. Res.*, vol. 13, pp. 448–455, 1963.

[62] J. S. Rankin, P. A. McHale, C. E. Artentzen, D. Ling, J. C. Greenfield, and R. W. Anderson, "The three-dimensional dynamic geometry of the left ventricle in the conscious dog," *Circ. Res.*, vol. 39, no. 3, pp. 304–313, Sept. 1976.

[63] R. W. Brower, H. T. ten Katen, and G. J. Meester, "Direct method for determining regional myocardial shortening after bypass surgery from radiopaque markers in man," *Amer. J. Cardiol.*, vol. 41, no. 7, pp. 1222–1229, June 1978.

[64] N. B. Ingels Jr., G. T. Daughters, E. B. Stinson, and E. L. Alderman, "Evaluation of methods for quantitating left ventricular segmental wall motion in man using myocardial markers as a standard," *Circulation*, vol. 61, no. 5, pp. 966–972, May 1980.

[65] G. D. Meier, A. A. Bove, W. P. Santamore, and P. R. Lynch, "Contractile function in canine right ventricle," *Amer. J. Physiol.*, vol. 239, no. 6, pp. H794–804, Dec. 1980.

[66] T. Arts, W. C. Hunter, A. S. Douglas, A. M. M. Muijtjens, J. W. Corsel, and R. S. Reneman, "Macroscopic three-dimensional motion patterns of the left ventricle," *Adv. Exp. Med. Biol.*, vol. 346, pp. 383–392, 1993.

[67] F. L. Villarreal, L. K. Waldman, and W. Y. W. Lew, "Technique for measuring regional two-dimensional finite strains in canine left ventricle," *Circ. Res.*, vol. 62, no. 4, pp. 711–721, Apr. 1988.

[68] A. A. Young and L. Axel, "Three-dimensional motion and deformation of the heart wall: Estimation with spatial modulation of magnetization—A model-based approach," *Radiology*, vol. 185, no. 1, pp. 241–247, Oct. 1992.

[69] C. C. Moore, W. G. O'Dell, E. R. McVeigh, and E. A. Zerhouni, "Calculation of three-dimensional left ventricular strains form biplanar tagged MR images," *J. Magn. Reson. Imag.*, vol. 2, no. 2, pp. 165–175, Mar. 1992.

[70] S. Kumar and D. Goldgof, "Automatic tracking of SPAMM grid and the estimation of deformation parameters from cardiac MR images," *IEEE Trans. Med. Imag.*, vol. 13, pp. 122–132, Mar. 1994.

[71] S. E. Fischer, G. C. McKinnon, M. B. Scheidegger, W. Prins, D. Meier, and P. Boesiger, "True myocardial motion tracking," *Magn. Res. Med.*, vol. 31, no. 4, pp. 401–413, Apr. 1994.

[72] A. A. Young, D. L. Kraitchman, L. Dougherty, and L. Axel, "Tracking and finite element analysis of stripe deformation in magnetic resonance tagging," *IEEE Trans. Med. Imag.*, vol. 14, pp. 413–421, Sept. 1995.

[73] T. S. Denney Jr. and J. L. Prince, "Reconstruction of 3D left ventricular motion from planar tagged cardiac MR images: An estimation theoretic approach," *IEEE Trans. Med. Imag.*, vol. 14, pp. 1–11, Dec. 1995.

[74] W. S. Kerwin and J. L. Prince, "Cardiac material markers from tagged MR images," *Med. Image Anal.*, vol. 2, no. 4, pp. 339–353, Dec. 1998.

[75] J. L. Prince and E. R. McVeigh, "Motion estimation form tagged MR image sequences," *IEEE Trans. Med. Imag.*, vol. 11, pp. 238–249, June 1992.

[76] S. C. Amartur and H. J. Vesselle, "A new approach to study cardiac motion: The optical flow of cine MR images," *Magn. Res. Med.*, vol. 29, no. 1, pp. 59–67, Jan. 1993.

[77] M. Tistarelli and G. Marcennaro, "Using optical flow to analyze the motion of human body organs from bioimages," in *Proc. Math. Meth. Biomed. Imag. Anal.*, Seattle, WA, USA, 1994, pp. 100–109.

[78] T. S. Denney Jr. and J. L. Prince, "Optimal brightness functions for optical flow estimation of deformable motion," *IEEE Trans. Imag. Processing*, vol. 3, pp. 178–191, Mar. 1994.

[79] ——, "A frequency domain performance analysis of Horn and Schunck's optical flow algorithm for deformable motion," *IEEE Trans. Imag Processing*, vol. 4, pp. 1324–1327, Sept. 1995.

[80] L. Dougherty, J. C. Asmuth, A. S. Blom, L. Axel, and R. Kumar, "Validation of an optical flow method for tag displacement estimation," *IEEE Trans. Med. Imag.*, vol. 18, pp. 359–363, Apr. 1999.

[81] S. S. Beauchemin and J. L. Barron, "The computation of optical flow," *ACM Comput. Surveys*, vol. 27, no. 3, pp. 444–467, Sept. 1995.

[82] S. M. Song and R. M. Leahy, "Computation of 3D velocity fields from 3D cine CT images of a human heart," *IEEE Trans. Med. Imag.*, vol. 10, pp. 295–306, Sept. 1991.

[83] S. M. Song, R. M. Leahy, D. P. Boyd, B. H. Brundage, and S. Napel, "Determining cardiac velocity fields and intraventricular pressure distribution from a sequence of ultrafast CT cardiac images," *IEEE Trans. Med. Imag.*, vol. 14, pp. 386–397, June 1994.

[84] J.-M. Gorce, D. Friboulet, and I. E. Magnin, "Estimation of three-dimensional cardiac velocity fields: Assessment of a differential method and application to three-dimensional CT data," *Med. Image Anal.*, vol. 1, no. 3, pp. 245–261, Mar. 1996.

[85] F. G. Meyer, R. T. Constable, A. J. Sinusas, and J. S. Duncan, "Tracking myocardial deformation using phase contrast MR velocity fields: A stochastic approach," *IEEE Trans. Med. Imag.*, vol. 15, pp. 453–465, Aug. 1996.

[86] A. A. Amini and J. S. Duncan, "Bending and stretching models for LV wall motion analysis from curves and surfaces," *Imag. Vis. Comput.*, vol. 10, no. 6, pp. 418–430, July 1992.

[87] S. K. Mishra, D. B. Goldgof, T. S. Huang, and C. Kambhamettu, "Curvature-based nonrigid motion analysis from 3D point correspondences," *Int. J. Image Syst. Tech.*, vol. 4, pp. 214–225, 1992.

[88] D. Friboulet, I. E. Magnin, C. Mathieu, A. Pommert, and K. H. Hoehne, "Assessment and visualization of the curvature of the left ventricle from 3D medical images," *Comput. Med. Imag. & Graph.*, vol. 17, no. 4–5, pp. 257–262, July 1993.

[89] C. Kambhamettu and D. B. Goldgof, "Curvature-based approach to point correspondence recovery in conformal nonrigid motion," *Comput. Vis. Graph. Imag. Processing*, vol. 60, no. 1, pp. 26–43, July 1994.

[90] S. Benayoun and N. Ayache, "Dense and nonrigid motion estimation in sequences of medical images using differential constraints," *Int. J. Comput. Vis.*, vol. 26, no. 1, pp. 25–40, Jan. 1998.

[91] H. Azhari, S. Sideman, J. L. Weiss, E. P. Shapiro, M. L. Weisfeldt, W. L. Graves, W. J. Rogers, and R. Beyar, "Three-dimensional mapping of acute ischemic regions using MRI: Wall thickening versus motion analysis," *Amer. J. Physiol.*, pt. 2, vol. 259, no. 5, pp. H1492–1503, Nov. 1990.

[92] A. M. Taratorin and S. Sideman, "3D functional mapping of left ventricular dynamics," *Comput. Med. Imag. Graph.*, vol. 19, no. 1, pp. 113–129, Jan. 1995.

[93] F. H. Sheehan, E. L. Bolson, H. T. Dodge, D. G. Mathey, J. Schofer, and H. K. Woo, "Advantages and applications of the centerline method for characterizing regional ventricular function," *Circulation*, vol. 74, no. 2, pp. 293–305, Aug. 1986.

[94] V. G. M. Buller, R. J. van der Geest, M. D. Kool, and J. H. C. Reiber, "Accurate three-dimensional wall thickness measurement from multislice short-axis MR imaging," in *Proc. IEEE Computers in Cardiology*. Los Alamitos, CA, Sept. 1994, pp. 245–248.

[95] E. L. Bolson and F. H. Sheehan, "Centersurface model for 3D analysis of regional left biventricular function," in *Proc. IEEE Computers in Cardiology*, London, U.K., Sept. 1993, pp. 735–738.

[96] E. L. Bolson, F. H. Sheehan, M. E. Legget, H. Jin, J. A. McDonald, P. D. Sampson, R. W. Martin, G. Bashein, and C. M. Otto, "Applying the centersurface model to 3-D reconstructions of the left ventricle for regional functional analysis," in *Proc. IEEE Computers in Cardiology*, Vienna, Austria, Sept. 1995, pp. 63–67.

[97] Y. C. Fung, *Biomechanics: Motion, Flow, Stress, and Growth*. New York: Springer Verlag, 1990.

[98] A. L. Yettram and C. A. Vinson, "Geometric modeling of the human left ventricle," *J. Biomech.*, vol. 101, pp. 221–223, 1979.

[99] A. L. Yettram, C. A. Vinson, and D. G. Gibson, "Computer modeling of the human left ventricle," *J. Biomech.*, vol. 104, no. 2, pp. 148–152, May 1982.

[100] A. A. Young, P. J. Hunter, and B. H. Smaill, "Epicardial surface estimation from coronary angiograms," *Comput. Vis. Graph. Imag. Processing*, vol. 47, no. 1, pp. 111–127, July 1989.

[101] F. G. Spinale, B. A. Carabello, and F. A. Crawford Jr., "Right ventricular function and three-dimensional modeling using computer-aided design," *J. Appl. Physiol.*, vol. 68, no. 4, pp. 1707–1716, Apr. 1990.

[102] A. Pentland and B. Horowitz, "Recovery of nonrigid motion and structure," *IEEE Trans. Pattern Anal. Machine Intell.*, vol. 13, pp. 730–742, July 1991.

[103] J. C. Cauvin, J. Y. Boire, M. Zanca, J. M. Bonny, J. Maublant, and A. Veyre, "3D modeling in myocardial 201TL SPECT," *Comput. Med. Imag. Graph.*, vol. 17, no. 4–5, pp. 345–350, July 1993.

[104] F. P. Czegledy and J. Katz, "A new geometric description of the right ventricle," *J. Biomed. Eng.*, vol. 15, no. 5, pp. 387–391, Sept. 1993.

[105] T. Gustavsson, R. Pascher, and K. Caidahl, "Model based dynamic 3D reconstruction and display of the left ventricle from 2D cross-sectional echocardiograms," *Comput. Med. Imag. Graph.*, vol. 17, no. 4–5, pp. 273–278, July 1993.

[106] M. S. Sacks, C. J. Chuong, G. H. Templeton, and R. Peshock, "*In vivo* 3-D reconstruction and geometric characterization of the right ventricular free wall," *Ann. Biomed. Eng.*, vol. 21, no. 3, pp. 263–275, May 1993.

[107] C. W. Chen, T. S. Huang, and M. Arrott, "Modeling, analysis, and visualization of left ventricle shape, and motion by hierarchical decomposition," *IEEE Trans. Pattern Anal. Machine Intell.*, vol. 16, pp. 342–356, Apr. 1994.

[108] S. Denslow, "An ellipsoidal shell model for volume estimation of the right ventricle from magnetic resonance images," *Acad. Radiol.*, vol. 1, no. 4, pp. 345–351, Dec. 1994.

[109] C. W. Chen, J. Luo, K. J. Parker, and T. S. Huang, "CT volumetric data-based left ventricle motion estimation: An integrated approach," *Comput. Med. Imag. Graph.*, vol. 19, no. 1, pp. 85–100, Jan. 1995.

[110] A. Goshtasby and D. A. Turner, "Segmentation of cardiac cine MR images for extraction of right and left ventricular chambers," *IEEE Trans. Med. Imag.*, vol. 14, pp. 56–64, Mar. 1995.

[111] A. Matheny and D. M. Goldgof, "The use of three- and four-dimensional surface harmonics for rigid and nonrigid shape recovery and representation," *IEEE Trans. Pattern Anal. Machine Intell.*, vol. 17, pp. 967–981, Oct. 1995.

[112] L. H. Staib and J. S. Duncan, "Model-based deformable surface finding for medical images," *IEEE Trans. Med. Imag.*, vol. 15, pp. 720–731, May 1996.

[113] E. Bardinet, N. Ayache, and L. D. Cohen, "Tracking and motion analysis of the left ventricle with deformable superquadrics," *Med. Image Anal.*, vol. 1, no. 2, pp. 129–150, June 1996.

[114] J. Declerck, J. Feldmar, and N. Ayache, "Definition of a four-dimensional continuous planisferic transformation for the tracking and the analysis of the left-ventricle motion," *Med. Image Anal.*, vol. 2, no. 2, pp. 197–213, June 1998.

[115] Y. Sato, M. Moriyama, M. Hanayama, H. Naito, and S. Tamura, "Acquiring 3D models of nonrigid moving objects from time and viewpoint varying image sequences: A step toward left ventricle recovery," *IEEE Trans. Pattern Anal. Machine Intell.*, vol. 19, pp. 253–259, Mar. 1997.

[116] E. A. Geiser, S. M. Lupkiewicz, L. G. Christie, M. Ariet, D. A. Conetta, and C. R. Conti, "A framework for three-dimensional time-varying reconstruction of the human left ventricle: Sources of error and estimation of their magnitude," *Comput. Biomed. Res.*, vol. 13, no. 3, pp. 225–241, June 1980.

[117] E. A. Geiser, M. Ariet, D. A. Conetta, S. M. Lupkiewicz, L. G. Christie Jr., and C. R. Conti, "Dynamic three-dimensional echocardiographic reconstruction of the intact human left ventricle: Technique and initial observations in patients," *Amer. Heart J.*, vol. 103, no. 6, pp. 1056–1065, June 1982.

[118] T. L. Faber, E. M. Stokely, R. M. Peshock, and J. R. Corbett, "A model-based four-dimensional left ventricular surface detector," *IEEE Trans. Med. Imag.*, vol. 10, pp. 321–329, Sept. 1991.

[119] D. Friboulet, I. E. Magnin, and D. Revel, "Assessment of a model for overall left ventricular three-dimensional motion from MRI data," *Int. J. Card. Imag.*, vol. 8, no. 3, pp. 175–190, Sept. 1992.

[120] W.-C. Huang and D. Goldgof, "Adaptive-size meshes for rigid and nonrigid analysis and synthesis," *IEEE Trans. Pattern Anal. Machine Intell.*, vol. 15, pp. 611–616, June 1993.

[121] T. L. Faber, C. D. Cooke, J. W. Peifer, R. I. Pettigrew, J. P. Vansant, J. R. Leyendecker, and E. V. Garcı a, "Three-dimensional displays of left ventricular epicardial surface from standard cardiac SPECT perfusion quantification techniques," *J. Nucl. Med.*, vol. 36, no. 4, pp. 697–703, Apr. 1995.

[122] G. Germano, H. Kiat, P. B. Kavanagh, M. Moriel, M. Mazzanti, H.-T. Su, K. F. van Train, and D. S. Berman, "Automatic quantification of ejection fraction from gated myocardial perfusion SPECT," *J. Nucl. Med.*, vol. 36, no. 11, pp. 2138–2147, Nov. 1995.

[123] G. Germano, P. B. Kavanagh, J. Chen, P. Waechter, H.-T. Su, H. Kiat, and D. S. Berman, "Operator-less processing of myocardial perfusion SPECT studies," *J. Nucl. Med.*, vol. 36, no. 6, pp. 2127–2132, Nov. 1995.

[124] T. McInerney and D. Terzopoulos, "A dynamic finite element surface model for segmentation and tracking in multidimensional medical images with application to 4D image analysis," *Comput. Med. Imag. Graph.*, vol. 19, no. 1, pp. 69–83, Jan. 1995.

[125] S. Ranganath, "Contour extraction from cardiac MRI studies using snakes," *IEEE Trans. Med. Imag.*, vol. 14, pp. 56–64, June 1995.

[126] H. K. Tu, A. Matheny, D. B. Goldgof, and H. Bunke, "Left ventricular boundary detection from spatio-temporal volumetric computed tomography images," *Comput. Med. Imag. Graph.*, vol. 19, no. 1, pp. 27–46, Jan. 1995.

[127] C. Nastar and N. Ayache, "Frequency-based nonrigid motion analysis: Application to four dimensional medical images," *IEEE Trans. Pattern Anal. Machine Intell.*, vol. 18, pp. 1067–1079, Nov. 1996.

[128] D. Rueckert and P. Burger, "Geometrically deformable templates for shape-based segmentation and tracking in cardiac MR image," in *Lecture Notes in Computer Science*. Venice, Italy: Springer-Verlag, 1997, vol. 1223, Energy MinImag. Meth. Comput. Vis. & Pattern Recogn..

[129] P. Shi, A. J. Sinusas, R. T. Constable, E. Ritman, and J. S. Duncan, "Point-tracked quantitative analysis of left ventricular surface motion from 3D image sequences: Algorithms and validation," *IEEE Trans. Med. Imag.*, vol. 19, pp. 36–50, Jan. 2000.

[130] J. S. Duncan, P. Shi, T. Constable, and A. Sinusas, "Physical and geometrical modeling for image-based recovery of left ventricular deformation," *Prog. Biophys. Mol. Biol.*, vol. 69, no. 1–2, pp. 333–351, 1998.

[131] J. Montagnat, H. Delingette, and G. Malandain, "Cylindrical echocardiographic image segmentation based on 3D deformable models," in *Lecture Notes in Computer Science*, 1999, vol. 1679, Medical Imaging Computing & Computer-Assisted Intervention, pp. 168–175.

[132] S. Biedenstein, M. Schäfers, L. Stegger, T. Kuwert, and O. Schober, "Three-dimensional contour detection of left ventricular myocardium using elastic surfaces," *Eur. J. Nucl. Med.*, vol. 26, no. 3, pp. 201–207, Mar. 1999.

[133] A. Yezzi, A. Tannenbaum, S. Kichenassamy, and P. Olver, "A gradient surface approach to 3-D segmentation," in *Proc. IS&T 49th Annu. Conf.*, Minneapolis, MN, May 1996.

[134] A. Yezzi, S. Kichenassamy, A. Kumar, P. Olver, and A. Tannenbaum, "A geometric snake model for segmentation of medical imagery," *IEEE Trans. Med. Imag.*, vol. 16, pp. 199–209, Apr. 1997.

[135] Y.-H. Tseng, J.-N. Hwang, and F. H. Sheehan, "Three-dimensional object representation and invariant recognition using continuous distance transform neural networks," *IEEE Trans. Neural Networks*, vol. 8, pp. 141–147, Jan. 1997.

[136] W. J. Niessen, B. M. ter Haar Romeny, and M. A. Viergever, "Geodesic deformable models for medical image analysis," *IEEE Trans. Med. Imag.*, vol. 17, pp. 634–641, Aug. 1998.

[137] B. P. F. Lelieveldt, R. J. van der Geest, M. R. Rezaee, J. G. Bosch, and J. H. C. Reiber, "Anatomical model matching with fuzzy implicit surfaces for segmentation of thoracic volume scan," *IEEE Trans. Med. Imag.*, vol. 18, pp. 231–238, Mar. 1999.

[138] L. L. Creswell, S. G. Wyers, J. S. Pirolo, W. H. Perman, M. W. Vannier, and M. K. Pasque, "Mathematical modeling of the heart using magnetic resonance imaging," *IEEE Trans. Med. Imag.*, vol. 11, pp. 581–589, Dec. 1992.

[139] J. S. Pirolo, S. J. Bresina, L. L. Creswell, K. W. Myers, B. A. Szabó, M. W. Vannier, and M. K. Pasque, "Mathematical three-dimensional solid modeling of biventricular geometry," *Ann. Biomed. Eng.*, vol. 21, no. 3, pp. 199–219, May 1993.

[140] E. Haber, D. N. Metaxas, and L. Axel, "Three-dimensional geometric modeling of cardiac right and left ventricles," presented at the Biomed. Eng. Soc. Annu. Meeting, San Diego, CA, 1997.

[141] ——, "Motion analysis of the right ventricle from MRI images," in *Computers in Cardiology*, vol. 1496, Medical Imaging Computing & Computer-Assisted Intervention, pp. 177–188.

[142] P. Shi, A. J. Sinusas, R. T. Constable, and J. S. Duncan, "Volumetric deformation analysis using mechanics-based data fusion: Application in cardiac motion recovery," *Int. J. Comput. Vis.*, vol. 35, no. 1, pp. 87–107, Nov. 1999.

[143] M. Kuwahara and S. Eiho, "3-D heart image reconstructed from MRI data," *Comput. Med. Imag. Graph.*, vol. 15, no. 4, pp. 241–246, July 1991.

[144] K. A. Bartels, A. C. Bovik, S. J. Aggarwal, and K. R. Diller, "The analysis of biological shape change from multidimensional dynamic images," *Comput. Med. Imag. Graph.*, vol. 17, no. 2, pp. 89–99, Mar. 1993.

[145] W. G. O'Dell, C. C. Moore, W. C. Hunter, E. A. Zerhouni, and E. R. McVeigh, "Three-dimensional myocardial deformations: Calculation with displacement field fitting to tagged MR images," *Radiology*, vol. 195, no. 3, pp. 829–835, June 1995.

[146] M. J. Moulton, L. L. Creswell, S. W. Downing, R. L. Actis, B. A. Szabo, M. W. Vannier, and M. K. Pasque, "Spline surface interpolation for calculating 3-D ventricular strains from MRI tissue tagging," *Amer. J. Physiol.*, pt. 2, vol. 270, no. 1, pp. H281–297, Jan. 1996.

[147] P. Radeva, A. A. Amini, and J. Huang, "Deformable B-solids and implicit snakes for 3D localization and tracking of SPAMM MRI data," *Comput. Vis. Image Underst.*, vol. 66, no. 2, pp. 163–178, May 1997.

[148] A. A. Young, "Model tags: Direct 3D tracking of heart wall motion from tagged MR images," *Med. Image Anal.*, vol. 3, no. 4, pp. 361–372, Dec. 1999.

[149] J. Huang, D. Abendschein, V. Davila, and A. A. Amini, "Four-dimensional LV tissue tracking from tagged MRI with a 4D B-spline model," *IEEE Trans. Med. Imag.*, vol. 18, pp. 957–972, Oct. 1999.

[150] X. Papademetris, P. Shi, D. P. Dione, A. J. Sinusas, R. T. Constable, and J. S. Duncan, "Recovery of soft tissue object deformation from 3D image sequences using biomechanical models," in *Lecture Notes in Computer Science*, A. Kuba, M. Sámal, and A. Todd-Pokropek, Eds. Berlin, Germany: Springer-Verlag, 1999, vol. 1613, Information Processing and Medical Imaging, pp. 352–357.

[151] ——, "Recovery of Soft Tissue Object Deformation from 3D Image Sequences Using Biomechanical Models," Image Processing and Analysis Lab., Dept. Diagnostic Radiology, Yale Univ., New Haven, CT, Tech. Rep.1999-01, June 1999.

[152] X. Papademetris, A. J. Sinusas, D. P. Dione, and J. S. Duncan, "3D cardiac deformation from ultrasound images," in *Lecture Notes in Computer Science*, vol. 1679, Medical Imaging Computing & Computer-Assisted Intervention, pp. 421–429.

[153] A. Pentland and S. Sclaroff, "Closed-form solutions for physically based shape modeling and recognition," *IEEE Trans. Pattern Anal. Machine Intell.*, vol. 13, pp. 703–714, July 1991.

[154] D. Metaxas and D. Terzopoulos, "Shape and nonrigid motion estimation through physics-based synthesis," *IEEE Trans. Pattern Anal. Machine Intell.*, vol. 15, pp. 580–591, June 1993.

[155] A. H. Barr, "Superquadrics and angle-preserving deformations," *IEEE Comput. Graph. Applicat.*, vol. 1, no. 1, pp. 11–23, Jan. 1981.

[156] C. W. Chen, J. B. Luo, and K. J. Parker, "Image segmentation via adaptive K-mean clustering and knowledge-based morphological operations with biomedical applications," *IEEE Trans. Imag. Processing*, vol. 7, pp. 1673–1683, Dec. 1998.

[157] J. J. Hopfield, "Neurons with graded responses have collective computational properties like those of two-state neurons," in *Proc. Nat. Acad. Sci.*, vol. 81, May 1984, pp. 3088–3092.

[158] O. Monga, R. Deriche, and J.-M. Rocchisani, "3D edge detection using recursive filtering: Application to scanner images," *Comput. Vis. Graph. Imag. Processing: Imag. Underst.*, vol. 53, no. 1, pp. 76–87, Jan. 1991.

[159] J. Declerck, J. Feldmar, M. L. Goris, and F. Betting, "Automatic registration and alignment on a template of cardiac stress and rest SPECT images," *IEEE Trans. Med. Imag.*, vol. 16, pp. 727–737, Dec. 1997.

[160] P. J. Besl and N. D. McKay, "A method for registration of 3D shapes," *IEEE Trans. Pattern Anal. Machine Intell.*, vol. 14, pp. 239–255, Feb. 1992.

[161] J. Feldmar and N. Ayache, "Rigid, affine and locally affine registration of free-form surfaces," *Int. J. Comput. Vis.*, vol. 18, no. 2, pp. 99–119, May 1996.

[162] T. W. Sederberg and S. R. Parry, "Free-form deformation of solid geometric models," *Proc. SIGGRAPH'86*, vol. 20, pp. 151–160.

[163] G. Germano and D. Berman, *Clinical Gated Cardiac SPECT*. Armonk, NY: Futura, 1999, ch. Quantitative gated perfusion SPECT, pp. 115–146.

[164] A. Goshtasby, "Design and recovery of 2-D and 3-D shapes using rational Gaussian curves and surfaces," *Int. J. Comput. Vis.*, vol. 10, no. 3, pp. 233–256, 1993.

[165] D. N. Metaxas, *Physics-Based Deformable Models: Applications to Computer Vision, Graphics and Medical Imaging*. Norwell, MA: Kluwer Academic, 1996.

[166] L. D. Cohen, "On active contour models and balloons," *Comput. Vis. Graph. Imag. Processing: Imag. Underst.*, vol. 53, no. 2, pp. 211–218, Mar. 1991.

[167] H. Delingette, "General object reconstruction based on simplex meshes," *Int. J. Comput. Vis.*, vol. 32, no. 2, pp. 111–146, Sept. 1999.

[168] M. Kass, A. Witkin, and D. Terzopoulos, "Snakes: Active contour models," *Int. J. Comput. Vis.*, vol. 1, no. 4, pp. 321–331, Jan. 1988.

[169] D. Terzopoulos, "Regularization of inverse visual problems involving discontinuities," *IEEE Trans. Pattern Anal. Machine Intell.*, vol. 8, pp. 413–424, Apr. 1986.

[170] J. Kittler and J. Illingworth, "Relaxation labeling algorithms—A review," *Imag. Vis. Comput.*, vol. 3, no. 4, pp. 206–216, Nov. 1985.

[171] D. F. Watson, "Computing the n-dimensional Delaunay tesselation with application to Voronoi polytopes," *Comput. J.*, vol. 24, no. 2, pp. 167–172, May 1981.

[172] A. Chakraborty, L. H. Staib, and J. S. Duncan, "Deformable boundary finding in medical images by integrating gradient and region information," *IEEE Trans. Med. Imag.*, vol. 15, pp. 859–870, Dec. 1996.

[173] E. Ekoulé, F. Peyrin, and C. Odet, "Description d'une procèdure de triangulation entièrament automatique," in *Proc. COGNITIVA 87*, Paris, France, pp. 88–95.

[174] F. H. Sheehan, E. L. Bolson, R. W. Martin, G. Bashein, and J. McDonald, "Quantitative three dimensional echocardiography: Methodology, validation and clinical applications," in *Lecture Notes in Computer Science*, vol. 1496, Medical Imaging Computing & Computer-Assisted Intervention, pp. 102–109.

[175] H. Hoppe, "Surface Reconstruction from Unorganized Points," Ph.D. dissertation, Univ. Washington, Seattle, WA, 1994.

[176] V. Caselles, F. Catté, T. Coll, and F. Dibos, "A geometric model for active contours in image processing," *Num. Mathematik.*, vol. 66, pp. 1–31, 1993.

[177] R. Malladi, J. Sethian, and B. Vemuri, "Shape modeling with front propagation: A level set approach," *IEEE Trans. Pattern Anal. Machine Intell.*, vol. 17, pp. 158–174, Feb. 1995.

[178] S. Osher and S. Sethian, "Fronts propagating with curvature dependent speed: Algorithms based on the Hamilton-Jacobi formalism," *J. Computat. Phys.*, vol. 79, pp. 12–49, 1988.

[179] Y.-H. Tseng, J.-N. Hwang, and F. H. Sheehan, "3-D heart modeling and motion estimation based on continuous distance transform neural networks and affine transform," *J. VLSI Signal Processing Syst. Signal, Imag., Video Technol.*, vol. 18, no. 3, pp. 207–218, Apr. 1998.

[180] A. J. Hanson, "Hyperquadrics: Smoothly deformable shapes with convex polyhedral bounds," *Comput. Vis. Graph. Imag. Processing*, vol. 44, no. 2, pp. 191–210, Nov. 1988.

[181] A. A. Requicha and H. B. Voelcker, "Solid modeling: A historical summary and contemporary assessment," *IEEE Comput. Graph. Applicat.*, vol. 2, no. 2, pp. 9–24, Mar. 1982.

[182] B. P. F. Lelieveldt, "Anatomical Models in Cardiovascular Image Analysis," Ph.D. dissertation, Leiden Univ. Med. Ctr., Leiden, The Netherlands, 1999.
[183] L. Piegl and W. Tiller, *The NURBS Book*, 2nd ed, Berlin, Germany: Springer-Verlag, 1996. Monographs in Visual Communication.
[184] K. A. Bartels, A. C. Bovik, and C. E. Griffin, "Spatio-temporal tracking of material shape change via multidimensional splines," in *Math. Meth. Biomed. Imag. Anal.*, Seattle, WA, 1994, pp. 110–116.
[185] J. M. Guccione and A. D. McCulloch, "Finite element modeling of ventricular mechanics," in *Theory of Heart*, P. J. Hunter, A. D. McCulloch, and P. Nielsen, Eds, Berlin, Germany: Springer-Verlag, 1991, pp. 122–144.
[186] A. A. Amini, Y. Chen, and D. Abendschein, "Comparison of land-mark-based and curved-based thin-plate warps for analysis of left-ventricular motion from tagged MRI," in *Lecture Notes in Computer Science*, vol. 1679, Medical Imaging Computing & Computer-Assisted Intervention, Berlin, Germany, pp. 498–507.
[187] E. Waks, J. L. Prince, and A. Douglas, "Cardiac motion simulator for tagged MRI," in *Math. Meth . Biomed. Imag . Anal.*, 1996, pp. 182–191.
[188] D. L. Kraitchman, A. A. Young, C.-N. Chang, and L. Axel, "Semiautomatic tracking of myocardial motion in MR tagged images," *IEEE Trans. Med. Imag.*, vol. 14, pp. 422–433, Sept. 1995.
[189] A. S. Douglas, W. C. Hunter, and M. D. Wiseman, "Inhomogeneous deformation as a source of error in strain measurements derived from implanted markers in the canine lef ventricle," *J. Biomech.*, vol. 23, no. 4, pp. 331–341, 1990.
[190] F. C. Schweppe, *Uncertain Dynamic Systems*. Englewood Cliffs, NJ: Prentice-Hall, 1973.
[191] T. S. Denney Jr. and E. R. McVeigh, "Model-free reconstruction of three-dimensional myocardial strain from planar tagged MR images," *J. Magn. Reson. Imag.*, vol. 7, no. 5, pp. 799–810, Sept. 1997.
[192] D. F. Leotta, B. Munt, E. L. Bolson, C. Kraft, C. M. Martin, R. W. amd Otto, and F. H. Sheehan, "Quantitative three-dimensional echocardiography by rapid imaging from multiple transthoracic windows: *In vitro* validation and initial *in vivo* studies," *J. Amer. Soc. Echocardiogr.*, vol. 10, no. 8, pp. 830–839, Oct. 1997.
[193] B. I. Munt, D. F. Leotta, E. L. Bolson, K. Coady, R. W. Martin, C. M. Otto, and F. H. Sheehan, "Left ventricular shape analysis from three-dimensional echocardiograms," *J. Amer. Soc. Echocardiogr.*, vol. 11, no. 8, pp. 761–769, Aug. 1998.
[194] S. Sasayama, H. Nonogi, M. Fujita, T. Sakurai, A. Wakabayashi, C. Kawai, S. Eiho, and M. Kuwahara, "Three-dimensional analysis of regional myocardial function in response to nitroglycerin in patient with coronary artery disease," *J. Amer. Coll. Cardiol.*, vol. 3, no. 5, pp. 1187–1196, May 1984.
[195] G. Germano, J. Erel, H. Lewin, P. B. Kavanagh, and D. S. Berman, "Automatic quantitation of regional myocardial wall motion and thickening from gated technetium-99n sestamibi myocardial perfusion single-photom emission computed tomography," *J. Amer. Coll. Cardiol.*, vol. 30, no. 5, pp. 1360–1367, Nov. 1997.
[196] A. A. Young, L. Axel, L. Dougherty, D. K. Bogen, and C. S. Parenteau, "Validation of tagging with MR imaging to estimate material deformation," *Radiology*, vol. 188, no. 1, pp. 101–108, July 1993.
[197] W. S. Kerwin and J. L. Prince, "Tracking MR tag surfaces using a spatiotemporal filter and interpolator," *Int. J. Image Syst. Technol.*, vol. 10, pp. 128–142, 1999.
[198] T. Arts, W. C. Hunter, A. Douglas, M. M. Muijtjens, and R. S. Reneman, "Description of the deformation of the left ventricle by a kinematic model," *J. Biomech.*, vol. 25, no. 10, pp. 1119–1127, Oct. 1992.
[199] J. Declerk, T. S Denney, C. Öztürk, W. O'Dell, and E. R. McVeigh, "Left ventricular motion reconstruction from planar tagged MR images: A comparison," *Phys. Med. Biol.*, vol. 45, no. 6, pp. 1611–1632, June 2000.
[200] J. Declerck, N. Ayache, and E. R. McVeigh, "Use of a 4D Planispheric Transformation for the Tracking and the Analysis of LV Motion with Tagged MR Images," INRIA, Sophia-Antipolis, France, Tech. Rep. 3535, Oct. 1998.
[201] C. Öztürk and E. R. McVeigh, "Four-dimensional B-spline based motion analysis of tagged cardiac MR images," in *Proc. SPIE*, vol. 3660, 1999, pp. 46–56.
[202] J. Lötjönen, P.-J. Reissman, I. E. Magnin, and T. Katila, "Model extraction from magnetic resonance volume data using a deformable pyramid," *Med. Image Anal.*, vol. 3, no. 4, pp. 387–406, Dec. 1999.
[203] T. F. Cootes, A. Hill, C. J. Taylor, and J. Haslam, "Use of active shape models for locating structures in medical images," *Imag. Vis. Comput.*, vol. 12, no. 6, pp. 355–365, July 1994.
[204] R. A. Greenbaum and D. G. Gibson, "Regional nonuniformity of left ventricular wall movement," *Br. Heart J.*, vol. 45, no. 1, pp. 29–34, Mar. 1981.
[205] E. Shapiro, D. L. Marier, M. G. St. J. Sutton, and D. G. Gibson, "Regional nonuniformity of wall dynamics in normal left ventricle," *Br. Heart J.*, vol. 45, no. 3, pp. 264–270, Mar. 1981.
[206] N. G. Pandian, D. J. Skorton, S. M. Collins, H. L. Falsetti, E. R. Burke, and R. E Kerber, "Heterogeneity of left ventricular segmental wall thickening and excursion in 2-dimensional echocardiograms of normal human subjects," *Amer. J. Cardiol.*, vol. 51, no. 10, pp. 1667–1673, June 1983.
[207] P. J. Besl and R. C. Jain, "Invariant surface characteristics for 3-D object recognition in range images," *Comput. Vis. Graph. Image Processing*, vol. 33, no. 1, pp. 33–80, Jan. 1986.
[208] P. Clarysse, D. Friboulet, and I. E. Magnin, "Tracking geometrical descriptors on 3-D deformable surfaces: Application to the left-ventricular surface of the heart," *IEEE Trans. Med. Imag.*, vol. 16, pp. 392–404, 1997.
[209] J. J. Koenderink and A. J. van Doorn, "Surface shape and curvature scales," *Imag. Vis. Comput.*, vol. 10, no. 8, pp. 557–565, Oct. 1992.
[210] C. Dorai and A. K. Jain, "Shape spectrum based view grouping and matching of 3D free-form objects," *IEEE Trans. Pattern Anal. Machine Intell.*, vol. 19, pp. 1139–1146, Oct. 1997.
[211] M. P. Do Carmo, *Differential Geometry of Curves and Surfaces*. Englewood Cliffs, NJ: Prentice-Hall, 1976.
[212] H. Azhari, E. Grenadier, U. Dinnar, R. Beyar, D. R. Adam, M. L. Marcus, and S. Sideman, "Quantitative characterization and sorting of three-dimensional geometries: Application to left ventricles *in vivo*," *IEEE Trans. Med. Imag.*, vol. 36, pp. 322–332, Mar. 1989.
[213] H. Azhari, S. Sideman, R. Beyar, E. Grenadier, and U. Dinnar, "An analytical descriptor of three-dimensional geometry: Application to the analysis of the left ventricle shape and contraction," *IEEE Trans. Biomed. Eng.*, vol. 34, pp. 345–355, May 1987.
[214] H. Azhari, I. Gath, R. Beyar, M. L. Marcus, and S. Sideman, "Discrimination between healthy and diseased hearts by spectral decomposition of their left ventricular 3D geometry," *IEEE Trans. Med. Imag.*, vol. 10, pp. 207–215, June 1991.
[215] M. A. Guttman, J. L. Prince, and E. R. McVeigh, "Tag and contour detection in tagged MR images of the left ventricle," *IEEE Trans. Med. Imag.*, vol. 13, pp. 74–88, Jan. 1994.
[216] M. A. Guttman, E. A. Zerhouni, and E. R. McVeigh, "Analysis and visualization of cardiac function from MR images," *IEEE Comput. Graph. Applicat.*, vol. 17, no. 1, pp. 55–63, Jan. 1997.
[217] L. Axel, D. Bloomgarden, C. N. Chang, D. Kraitchman, and A. A. Young, "SPAMMVU: A program for the analysis of dynamic tagged MRI," in *Proc. ISMRM*, 1993, p. 724.
[218] A. Bazille, M. A. Guttman, E. R. McVeigh, and E. A. Zerhouni, "Impact of semiautomated versus manual image segmentation errors on myocardial strain calculation by MR tagging," *Inv. Rad.*, vol. 29, no. 4, pp. 427–433, Apr. 1994.
[219] S. Zhang, M. A. Douglas, L. Yaroslavsky, R. M. Summers, V. Dilsizian, L. Fananapazir, and S. L. Bacharach, "A Fourier based algorithm for tracking SPAMMM tags in gated magnetic resonance cardiac images," *Med. Phys.*, vol. 23, no. 8, pp. 1359–1369, Aug. 1996.
[220] W. S. Kerwin and J. L. Prince, "The Kriging update model and recursive space-time function estimation," *IEEE Trans. Signal Processing*, vol. 47, pp. 2942–2952, Nov. 1999.
[221] *Handbook of Applied Advanced Geostatistical Ore Reserve Estimation*, Elsevier Sci., Amsterdam, The Netherlands, 1988.
[222] N. F. Osman, W. S. Kerwin, E. R. McVeigh, and J. L. Prince, "Cardiac motion tracking using CINE harmonic phase (HARP) magnetic resonance imaging," *Magn. Res. Med.*, vol. 42, no. 6, pp. 1048–1060, Dec. 1999.
[223] J. Garot, D. A. Bluemke, N. F. Osman, C. E. Rochitte, E. R. McVeigh, E. A. Zerhouni, and J. L. Prince, "Fast determination of regional my ocardial strain fields from tagged cardiac images using harmonic phase MRI," *Circulation*, vol. 101, no. 9, pp. 981–988, Mar. 2000.
[224] N. F. Osman and J. L. Prince, "Motion estimation from tagged MR images using angle images," *Int. Conf. Image Processing*, vol. 1, pp. 704–708, 1998.
[225] ——, "Visualizing myocardial function using HARP MRI," *Phys. Med. Biol.*, vol. 45, no. 6, pp. 1665–1682, June 2000.
[226] C. Taylor and A. Colchester, Eds., "Medical Imaging Computing & Computer-Assisted Intervention," in *Lecture Notes in Computer Science*, Cambridge, U.K.: Springer-Verlag, Oct. 1999, vol. 1679.
[227] A. Colchester, W. M. Wells, and S. Delp, Eds., "Medical Imaging Computing & Computer-Assisted Intervention," in *Lect. Notes Comput. Sci.*. Boston, MA: Springer-Verlag, Sept. 1998, vol. 1496.